

Solar Driven Desalination of Seawater by Self-floating MoSe₂ Based Membranes



Syed Muhammad Murtaza Sherazi

Reg. No 331168

A thesis presented as partial fulfilment of the requirements for the degree of

Master of Science in Chemistry

Supervised by: Dr. Muhammad Adil Mansoor

Department of Chemistry

School of Natural Science

National University of Sciences and Technology

H-12, Islamabad, Pakistan 2023

THESIS ACCEPTANCE CERTIFICATE

Certified that final copy of MS thesis written by Syed Muhammad Murtaza Sherazi (Registration No. 00000331168), of School of Natural Sciences has been vetted by undersigned, found complete in all respects as per NUST statutes/regulations, is free of plagiarism, errors, and mistakes and is accepted as partial fulfillment for award of MS/M.Phil degree. It is further certified that necessary amendments as pointed out by GEC members and external examiner of the scholar have also been incorporated in the said thesis.


Signature: 

Name of Supervisor: Dr. M. Adil Mansoor

Date: 25/08/23

Signature (HoD): 


Date: 25/8/23

Signature (Dean/Principal): 

Date: 29.8.2023

National University of Sciences & Technology**MS THESIS WORK**

We hereby recommend that the dissertation prepared under our supervision by: Syed Muhammad Murtaza Sherazi, Regn No. 00000331168 Titled: Solar Driven Desalination of Seawater by Self-Floating MoSe₂ Based Membranes be Accepted in partial fulfillment of the requirements for the award of **MS** degree.

Examination Committee Members1. Name: DR. FAHEEM AMINSignature: 2. Name: DR. SHAHID IQBALSignature: Supervisor's Name DR. M. ADIL MANSOORSignature: Co-Supervisor's Name PROF. MANZAR SOHAILSignature: 


Head of Department

25/8/23
Date

COUNTERSIGNEDDate: 29.08.2023


Dean/Principal

Acknowledgements

I want to start by giving Allah, the Almighty, praise for his blessings on me and for giving me the stamina to finish my degree. God bless the Holy Prophet, Hazrat Muhammad (SAW) and his progeny. I also want to express my gratitude to everyone who helped me along the way.

I would like to express my gratitude to my parents and siblings for their support and prayers, without which my success would not have been possible.

I would really like to acknowledge my supervisor, **Dr. Muhammad Adil Mansoor**, from the bottom of my heart for all of his support and encouragement. Throughout my MS, he mentored me and helped me with every issue. He was available at all times to guide and assist his students. He has my gratitude.

I would like to express my deepest gratitude to my co-supervisor, **Prof. Manzar Sohail**. He not only provided me with academic guidance but also served as a mentor, offering valuable insights and constructive feedback that greatly enriched my understanding of the subject matter. Their dedication and commitment to my research goals were truly remarkable, and I am profoundly grateful for their patience and encouragement throughout this process. Their unwavering support, guidance, and expertise have been instrumental in shaping the outcome of this work.

I am grateful to GEC members **Dr. Shahid Iqbal** and **Dr. Faheem Amin** for their assistance during my research. They helped me with my research and directed me at every turn.

Many thanks to all of my lab, class, and research colleagues. I would especially like to thank Muhammad Fiaz, Muhammad Saad, Kainat Fatima, Sara Zainab, Komal Zafar, Hamna Hafeez, Muhammad Abdullah, Umair Lateef, Muhammad Nauman, Touqir Hussain, Javeria Tabassum, Hammad Nasir, Safdar Ali, Muhammad Ali, Abrar Hussain, Asad Asghar, Ghulam Murtaza and Naeem Abbas for helping me with my research and for acting in a kind and courteous manner.

Syed Muhammad Murtaza Sherazi

Abstract

Employing solar energy for the interfacial desalination of seawater via nanoparticles presents a sustainable and eco-friendly solution to alleviate the global water scarcity problem. Traditional desalination methods often suffer from low efficiencies, and the majority necessitate extensive heating, making them economically unfavorable. This study presents a facile hydrothermal synthesis of MoSe_2 , CoMoSe_2 , and NiMoSe_2 nanoparticles. These particles are subsequently deposited onto a cotton gauze membrane using a straightforward procedure. Characterization of the formed nanoparticles was performed using various analytical techniques such as X-ray diffraction (XRD), Scanning electron microscopy (SEM), Energy dispersive spectroscopy (EDS), UV-Visible spectroscopy, and Raman Spectroscopy. The hydrophilic nature of the membrane surface was verified through contact angle measurements, while its photothermal conversion efficiency was confirmed via infrared imaging. We conducted multiple tests to calculate the photothermal evaporation rate and solar efficiency to assess stability. The desalinated water produced through this solar method was subsequently tested for ion concentration using atomic absorption spectroscopy, which yielded results below the drinking water standard set by the World Health Organization. As a result, we have successfully synthesized a porous, hydrophilic, and self-floating membrane that shows promise for real-world implementation.

Table of Contents

Table of Equations	VI
1. Introduction	1
1.1 Background:	1
1.2 Problem Statement	1
1.3 Desalination Methods	2
1.3.1 Membrane Distillation Methods:	3
1.3.2 Thermal Distillation	4
1.4 Solar Stills	6
1.5 Role of Nanotechnology and membrane nanotechnology	6
1.5.1 Effect of metal chalcogenide nanoparticles on membrane.....	7
1.6 Plasmonic Heating Effect:	9
1.6 Parameters for the assessment of desalination of seawater	9
1.6.1 Flux	10
1.6.2 Solar Efficiency.....	10
1.7 Contact Angle	11
1.7.1 Hydrophilic surface.....	12
1.7.2 Hydrophobic surface	12
1.7.3 Superhydrophobic surface.....	12
1.7.4 Contact angle measurement	12
1.8 IR imaging Technology	12
1.9 Substrates	13
1.10 Objectives of Research	13
2. Literature Review	15
3. Experimental	25
3.1 Materials Required for Synthesis:	25
3.2 Synthesis of Molybdenum Selenide:.....	25
3.3 Synthesis of Nickel-Doped Molybdenum Selenide:	26
3.4 Synthesis of Cobalt-Doped Molybdenum Selenide:	27
3.5 Preparation of Nanoparticle-Embedded Cotton Gauze Membranes:	28
3.6 Indoor Desalination Experiment	30

3.7 Outdoor Desalination Experiment	31
3.8 Indoor Experiments in Absence of Light	32
4. Results and Discussion	33
4.1 Material characterization of all the prepared MoSe ₂ , NiMoSe ₂ and CoMoSe ₂	33
4.2 Mechanism of Plasmonic Resonance.....	40
4.3 Evaporative and Photothermal Efficiencies of the Evaporating Device	40
4.4 Contact Angle Measurement:.....	41
4.5 Photothermal Conversion Performance:	42
4.5.1 Evaporative Performance under one Solar Radiation:	42
4.5.2 Evaporative Performances at Room Conditions:	43
4.6 Solar Efficiencies of the Materials:.....	43
4.7 Photothermal Efficiencies measurement using IR imaging:	45
4.8 Stability	49
5. CONCLUSION	51
6. REFERENCES	52

Table of Figures

Figure 1: Summary of Desalination methods [6]	3
Figure 2: Solar Distillation Unit.....	5
Figure 3: Classes of Nanomaterials [7].....	7
Figure 4: Contact Angle.....	12
Figure 5: MoSe ₂ Synthetic Scheme	26
Figure 6: NiMoSe ₂ Synthetic Scheme.....	27
Figure 7: CoMoSe ₂ Synthetic Scheme	28
Figure 8: XRD Spectra Of MoSe ₂ , CoMoSe ₂ and NiMoSe ₂	33
Figure 9: SEM images of (a) MoSe ₂ , (b) CoMoSe ₂ , (c) NiMoSe ₂ , (d) MoSe ₂ @CG, (e) CoMoSe ₂ @CG and (f) NiMoSe ₂ @CG.....	38
Figure 10: Tauc Plot of MoSe ₂	38
Figure 11: Tauc Plot of CoMoSe ₂	39
Figure 12: Tauc plot of NiMoSe ₂	39
Figure 13: Water contact angles of (b) Cotton Gauze, (c) MoSe ₂ @CG, (d) CoMoSe ₂ @CG and (e) NiMoSe ₂ @CG.....	42
Figure 14: Evaporation Flux	43
Figure 15: Solar Efficiencies	45
Figure 16: Photothermal efficiencies	46
Figure 17: IR images of (a) MoSe ₂ , (b) CoMoSe ₂ and (c) NiMoSe ₂	49
Figure 18: Stability Check.....	50

Table of Equations

Equation 1: Equation for Finding Water Flux	10
Equation 2: Equation for Solar Efficiency	10
Equation 3: Equation for finding Latent Heat of Vaporization.....	11
Equation 4: Debye Scherrer Equation.....	34

1. Introduction

1.1 Background:

Water is a basic human need, and although the planet is about 70 % covered with it (1.4×10^9 km³), there is still a significant drinking water scarcity in many nations due to a lack of fresh, potable water. Accessible saltwater has an average salinity of 35000 ppm, or mg/L. Only 2.5 % of the total amount of water is available as fresh water, and of that, 80 % is trapped in glaciers, leaving only 0.5 % of fresh drinking water.[1] A higher rate of extraction is predicted compared to water recharge due to the growing urbanisation of the population. As a result, 40 % of the world's population currently experiences water scarcity, and it is predicted that this percentage could rise to 60 % by the year 2025.

1.2 Problem Statement

Many parts of the world are experiencing a lack of fresh drinking water as a result of the dwindling groundwater basins. Alternative water sources including desalination, recycling, water importation, etc., have become popular in many places. Desalination is the process of removing salt from saltwater with salinities up to 35000 ppm[2] and bringing them down to the 500 ppm i.e., WHO drinking water standard. Desalination has been practiced for centuries, but recently it has become more popular. Saudi Arabia, which is at the top of the list and meets 60 % of the world's water demand through desalination, is one of many nations that entirely rely on desalinated water. The desalination method is also used in Qatar and Kuwait to produce all of their water needs.[3]

1.3 Desalination Methods

The recently used methods of water filtration include solar distillation, forward osmosis, and reverse osmosis. The two desalination methods are as follows:

1.3.1 Membrane Distillation

1.3.2 Thermal Distillation

Several different desalination methods are used in these two processes:

The methods included in membrane distillation are,

- i. Electrodialysis (ED),
- ii. Electrodialysis reversal (EDR),
- iii. Reverse osmosis (RO) [4]

The thermal distillation process includes,

- i. Multistage flash distillation (MSF)
- ii. Multi-effect distillation (MED)
- iii. Vapor compression distillation (VCD)
- iv. Solar distillation [5]

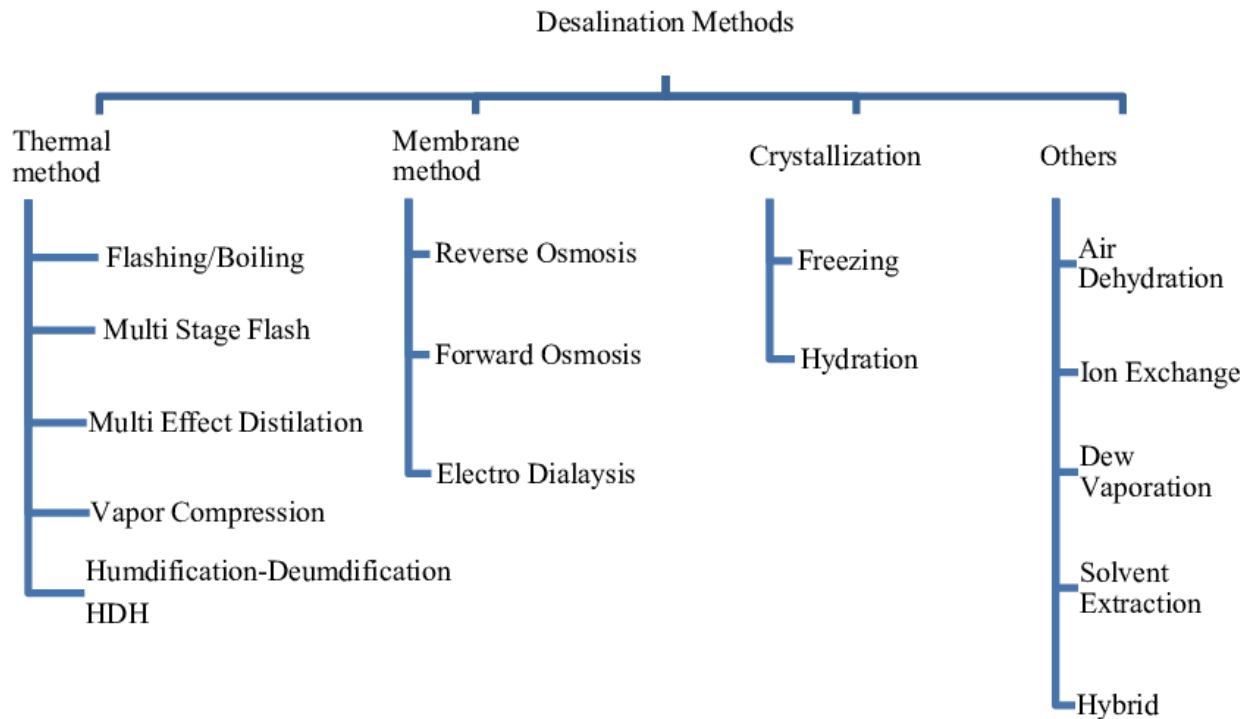


Figure 1: Summary of Desalination methods [6]

1.3.1 Membrane Distillation Methods:

Membrane distillation is a technique where the distillation process is carried out using a membrane and a driving force. Depending on the kind of membrane distillation being used, the driving source can be an electrical potential or a pressure gradient.

1.3.1.1 Electrodialysis and Reverse Electrodialysis:

Only positively or negatively charged ions are permitted to flow across the membranes used in these techniques, therefore only a positive or a negative ion can do so. Na, Cl, Cd, and carbonates are the four ions that are most frequently found in saline water. On one side, fresh water is produced via these processes, which utilize electrical potential to drive a particular ion through the membrane. Anions, which are negatively charged ions, are directed to the positively charged cathode, whereas cations, which are positively charged ions, are drawn to the negatively charged anode. When the membranes are in place, some membranes only permit cations and some

only permit anions to pass. They can efficiently extract the components from the saline water in this way. The reversal electrolysis serves the same purpose as electrolysis, with the difference that the electrode charge and polarity are regularly altered. The scaling and debris can be eliminated in this manner.

1.3.1.2 Reverse Osmosis:

In this procedure, the saline water is forced at a very high pressure across the membrane, allowing only the pure water to pass and preventing the salt ions from doing so. Following reverse osmosis, many membrane types, including nano-, micro-, and ultra-filtration, are used. Due to the narrow membrane pores, reverse osmosis pretreats the water chemically to prevent biological growth. Additionally, this type of membrane physically stops the solid particles.

All these techniques are highly effective and energy-efficient, but fouling is their biggest drawback. These evaporation devices also have issues with difficult procedures, low efficiency, and limited reusability. These disadvantages encourage the development of a new kind of membrane.

1.3.2 Thermal Distillation

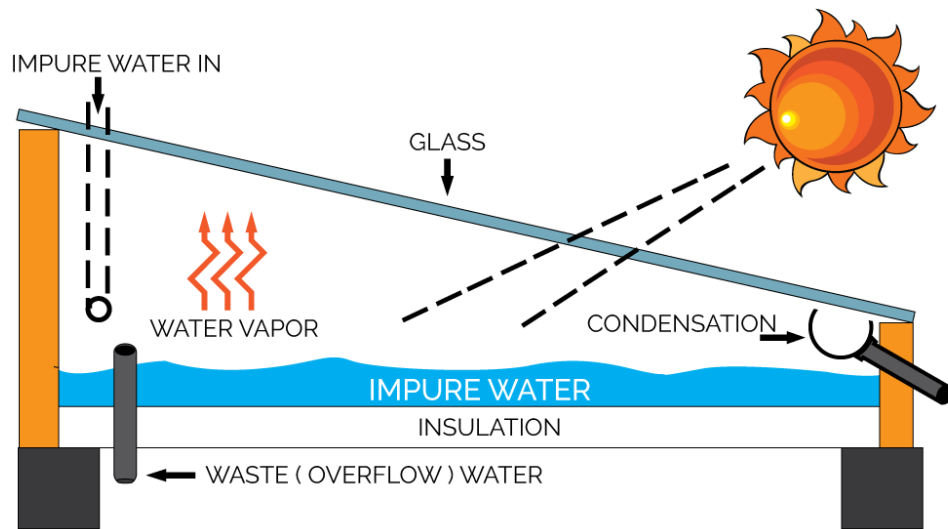
1.3.2.1 Vapour Compression Distillation

We can use this process in conjunction with other processes. As the vapours are condensed, the feed water is evaporated using the heat that is released. Most of the time, this technology is employed for the medium- to small-scale production of drinking water in places like resorts, factories, and other petroleum drilling sites.

1.3.2.2 Solar Distillation

The process of using solar energy to create fresh water from salt water is known as solar distillation, as the name suggests. Through a glass container, the solar radiation falls on the saline water, allowing it to evaporate as pure water vapours while leaving the salts and other contaminants behind. The water that has evaporated is caught in the condensate trough after condensing on the

tilted glass wall. The glass or plastic covering benefits by serving as a source of light transmission as well as a surface for attaching and collecting condensed water. The remaining water can be properly disposed. This approach is typically employed in areas with limited access to freshwater sources, and the amount of water it produces relies on the design and location. A survey in Texas found that 7.5 square feet of surface area can provide enough water for one person to survive.



Solar Distillation Of Water

Figure 2: Solar Distillation Unit

1.3.2.3 Multi-stage Flash Distillation

The seawater is run through several chambers throughout this process. The water is heated to a very high temperature to boil, and a high pressure is applied. When the pressure is decreased to a very low level, the water boils even more quickly. Condensation occurs, and the clean water vapours are collected.

1.3.2.4 Multi-effect Distillation

The only difference between this technique and the one above is the quantity of vessels. In the MSF process, a single chamber is utilised, but in the MED process, multiple vessels are utilised.

The water is condensed and collected more successfully because of using multiple vessels.

1.4 Solar Stills

Solar stills had been developed centuries ago. As fossil fuels are becoming more expensive to produce energy from, there is a rising demand for thermal desalination technology. There is also a demand for small-scale desalination systems in isolated places where fresh water is scarce. Desalination systems powered by solar energy are therefore preferred for supplying a dependable source. Renewable energy and desalination technologies may be the most effective combinations for this use. These have a low production cost for pure water. Solar energy is the most promising energy source for desalination in terms of thermal energy. In order to convert solar energy into thermal energy for solar desalination processes, the technology typically consists of a renewable thermal energy source, solar energy absorbers, evacuated tubes, and flat plate solar collectors. There are two ways to accomplish this. The first method uses solar stills, in which the energy from the sun falls directly on the salt water, and the second uses solar collectors, in which the energy from the sun is first collected and then transferred to the salt water.

1.5 Role of Nanotechnology and membrane nanotechnology

Nanotechnology works with particles that are 1–100 nm in size. An emerging field called nanotechnology can synthesize materials from a bottom-up approach. Smaller size increases surface area, which improves particle performance and raises the possibility of better functionality. As a result, desalination has improved in terms of its economic stability. Less chemicals are required on the membranes, thus there are fewer environmental problems. These kinds of nanomembranes are frequently referred to as "nano-enabled membranes" since the chemical and

physical characteristics of the membranes are largely determined by the structure of the membranes and the chemical(s) used. In both research and industry, these membranes are achieving breakthroughs because of their exceptional productivity and high salt rejection rates. The evidence for various nanoparticles and their nanocomposites, which offer many paths for sustainable development, is provided by quantum leaps. This offers a positive path toward the development of accessible, cost-effective, and sustainable solutions to the freshwater shortage dilemma. Nanotechnology can therefore solve this issue and advance the development of desalination technology.

The desalination of saltwater has undergone a revolution because of the combination of nanotechnology and membranes. Membranes with nanotechnology enhancements speed up the generation and separation of water considerably while lowering startup costs and operating costs.

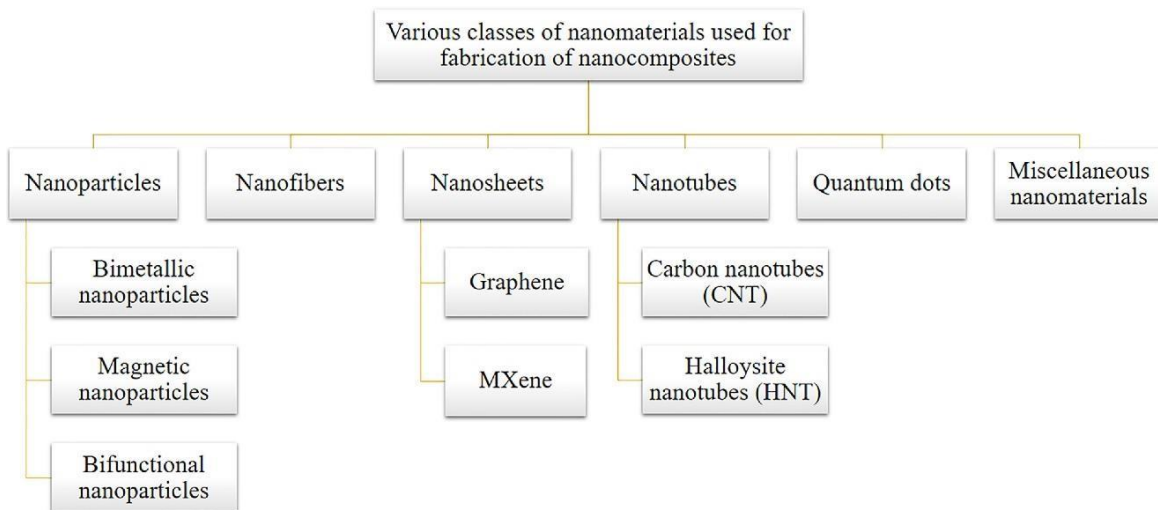


Figure 3: Classes of Nanomaterials [7]

1.5.1 Effect of metal chalcogenide nanoparticles on membrane

The most effective conversion method is now liquid to gas conversion. Solar efficiency for bottom heating ranges from 30 to 45 percent, whereas interfacial evaporation can boost it to 64 percent.

As the heat is localised, interfacial heating is better than the traditional techniques like bottom heating and volumetric heating.

The substrate prevents bottom heating by allowing water vapour to escape from the top layer, which absorbs solar radiation and transforms it into thermal energy. When Nanoparticles are assembled with a substrate, heat dissipation is restricted, which results in a temperature difference between the top layer and bottom water. Such membranes can be manufactured by the use of nanotechnology. Nanodots, Graphene oxide, CNTs, and polymer combinations, and metal dichalcogenides membranes are examples of nanomaterials that can be used.

Since nanoparticles are excellent light absorbers and have optical, photothermal, and electrochemical capabilities, they may efficiently convert light to heat and readily produce water vapour. This process is known as the plasmonic resonance effect, and it is generated by solar light.

Due to their improved light-absorbing properties, nanoparticles are better at absorbing light than bulk materials. It is more practical to restrict nanoparticles on the water's surface since dispersing nanoparticles in bulk water demands a large concentration of nanoparticles. Only an average amount of nanofluids causes the absorption and scattering, which lengthens the average path and transfers heat to the water for evaporation, while a very large concentration induces near saturation.

Bandgaps in chalcogenides are large. Rather than occurring at values of the indirect bandgap, which do not require the phonon support for the solar absorption, most of the dominant transition happens at the direct bandgap.

Typically, a tauc plot is used to assess the optical properties of the nanoparticles, such as absorption, transmittance, and reflectance, in order to determine their band gap. Spectroscopy in the UV and visible range is used to measure these properties.

Selenium and Molybdenum exhibit a surface plasmonic effect. When bimetallic nanoparticles are synthesized, the band gap reduces. Gold and silver nanoparticles are the most effective for surface plasmonic effect, and extensive research has previously been done on these nanoparticles. Silver has the best potential to display surface plasmonic effect among them, but due to the existence of chloride ions, silver is not as stable as gold. Although it can also generate heat, aluminium is unstable, exactly as silver metal. We are working on less expensive, more readily available materials because these ones are expensive. The form and size of the nanoparticles affect the surface plasmonic effect. In metal chalcogenides, plasmonic resonance typically occurs on localised surfaces, and this effect can be strengthened by doping, which produces holes or raises the charge density.

1.6 Plasmonic Heating Effect:

Metal nanoparticles can produce heat when illuminated optically. The incident photons are absorbed by the metal nanoparticles during this process, and heat is then transmitted to the surroundings. Due to the availability of free mobile electrons in metal nanoparticles, this reaction is mostly observed in these particles. The optical absorption rate can be used to determine how much heat is being released because metals do not emit much light. It is also difficult to see the surface temperature increase. The transfer of optical illumination into the metal nanoparticles, where the mobile electrons are excited, is necessary for the processes of heat diffusion into the environment. When the mobile electrons are de-excited, heat is released into the environment. In the case of plasmon resonance, the heat generating mechanism is clearly visible. The aggregate motion of many electrons is known as plasmon resonance.[7]

1.6 Parameters for the assessment of desalination of seawater

The desalination activity is affected by various factors, some are described below.

1.6.1 Flux

Flux is typically used to represent how quickly water passes through a membrane. By using the following equation as a formula, the water evaporation rate by the solar-driven evaporator device can be determined.

$$E_w = \frac{\Delta m}{A \cdot t}$$

Equation 1: Equation for Finding Water Flux

In the equation above, m stands for the mass of the water that is evaporated in kilograms, t for the amount of time in hours that the evaporation took place, and A for the device's area in square meters. E_w is therefore measured in $\text{kg m}^{-2}\text{h}^{-1}$.

1.6.2 Solar Efficiency

The solar efficiency of photothermal evaporating device can be determined by the equation.

$$\eta = \frac{m h_{lv}}{C_{opt} q_i}$$

Equation 2: Equation for Solar Efficiency

While m is the mass loss of water owing to evaporation from the water surface as a result of solar radiation, η stands for the solar efficiency of solar to thermal conversion. By subtracting the mass loss from the water surface during the same period of time in the absence of solar light irradiation, the m is calculated. Latent enthalpy of vaporization from liquid to gas conversion and sensible heat H_s are combined to form H_{lv} .

1.6.2.1 Sensible Heat, H_s

Heat is what changes the body or system temperature; it does not affect the system state or produce a phase shift, for example, it heats the water but does not melt the ice. In photothermal desalination,

solar light causes a localised system, such as a nanoparticle membrane on the water surface, to alter in temperature. It is measured in kW.

1.6.2.2 Latent Heat of Vaporization, H_{lv}

It is the amount of heat needed to convert one mole of a liquid into a gas at standard atmospheric pressure when the liquid is at its boiling point. It measures in kg/mol or kJ/kg. Water has an H_{lv} of 2,260 kJ/kg. Temperature variations cause a change in the heat of vaporisation. H_{lv} changes at various temperatures, as indicated by the given equation.

$$h_{lv} = \alpha + \beta T + \gamma T^{1.5} + \delta T^{2.5} + \epsilon T^3$$

Equation 3: Equation for finding Latent Heat of Vaporization

1.7 Contact Angle

The contact angle is a qualitative indicator of how well a liquid will wet a solid's surface. The characteristics of the surface as well as the fluid's surface tension have an impact on the shape of the drop that forms on the solid's surface. Due to surface tension, the drop adopts the curved shape at the boundary between the gaseous phase and the liquid. The contact angle arises between the solid/liquid surface and the tangent to the gaseous/liquid interface as the edge points and the contour merges into the solid bearing surface. It is typically used to analyse the wettability of surface.

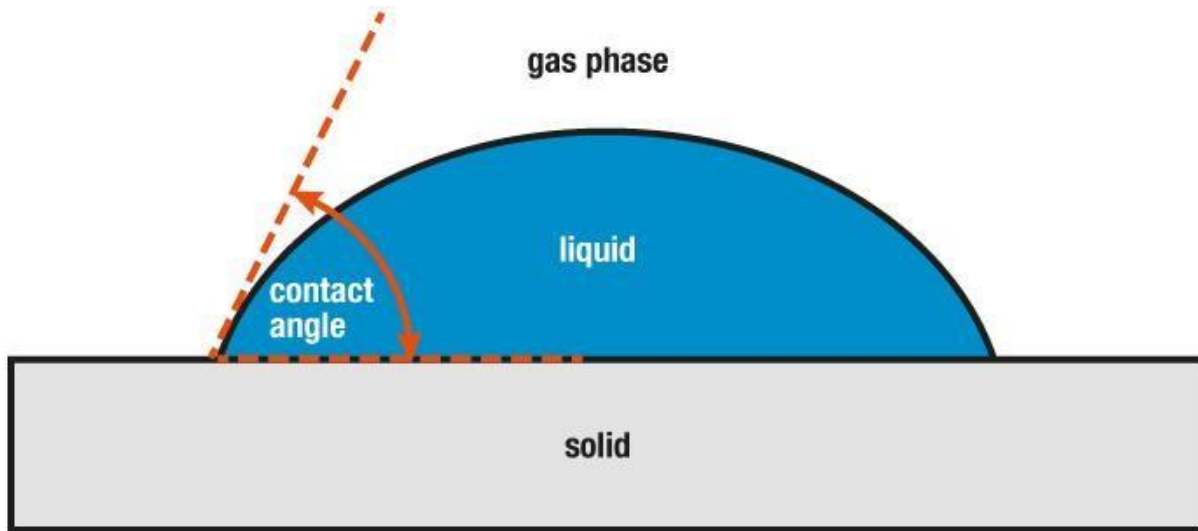


Figure 4: Contact Angle

1.7.1 Hydrophilic surface

The surface is wettable if a liquid drop hits a solid surface, spreads evenly, and displays a 0° contact angle. The surface is wettable and hydrophilic when the contact angle ranges from 0° to 90° .

1.7.2 Hydrophobic surface

A surface is considered hydrophobic and completely unwettable if the surface contact angle is between 90° and 180° .

1.7.3 Superhydrophobic surface

A surface is said to be ultra-hydrophobic if the contact angle is more than 180 degrees. It absolutely repels liquids. The lotus effect is another name for this phenomenon.

1.7.4 Contact angle measurement

Contact angle measurement is the qualitative technique for identifying a surface's hydrophobic or hydrophilic properties.

1.8 IR imaging Technology

Infrared imaging technology is typically used to determine an object's temperature. The majority of the electromagnetic radiation emitted by objects are in the infrared (IR) wavelength range, that

are not visible with the naked eyes. In comparison to a cool object, a hotter object emits more infrared radiation.

1.9 Substrates

Substrates are the materials that can be utilised as a water transport medium in the solar evaporation device used in the desalination process as well as a thermal insulator. These supporting material characteristics are also necessary for the solar evaporation processes. The substrate must have excellent thermal insulation, high light absorption in the solar spectrum, floating capability, light weight, and water transport qualities in order to be used in solar evaporation devices. According to the literature, materials like wood, cellulose foam, polystyrene, and polyurethane have demonstrated strong thermal insulating capabilities for interfacial evaporation and are easily floatable. As a floating substrate material for this study, we employed cotton gauze and a regular dishwashing sponge. Cellulosic cotton gauze is a lightweight, porous, low-cost material that may float on the water and has a low heat conductivity. Additionally, as seen in those graphs, the cotton gauze exhibits interaction in the corresponding IR spectra when the particles are deposited on it.

1.10 Objectives of Research

Due to the lack of fresh drinking water and the fact that 97 % of the world's water is found in oceans, many countries are experiencing water scarcity concerns. There is no way to drink this water. Therefore, various methods have been developed to turn this saline water into pure water. Every technique is costly. Resources in the world are running out every day. Some techniques, like bulk heating, demand a lot of heat, but they're not all that efficient. Other processes rely on membranes and changing those membranes after a short while costs a lot of money. Recent advances in nanotechnology have paved the way to synthesize photothermal membranes, which can evaporate water by using sunlight and can float on the surface.

The major goal of this research is to develop nanoparticles that can float on the water's surface and have a high photothermal absorption efficiency. Such features are present in metal chalcogenides. These nanoparticles are simple to produce, exhibit a wide range of band gaps, and can function as photocatalysts. When applied to any substrate, the nanoparticles can boost the water flux, such that the ecologically friendly way of employing solely solar light can be used to enable large-scale production.

2. Literature Review

In a research, researchers described a sizable section of CuS/PE porous membrane that displayed interfacial photothermal plasmonic transformation to heat. The entire sunlight spectrum was successively absorbed by the membrane. The membrane is hydrophilic by nature, has a high porosity, low thermal conductivity, and can float on water. With a water flux of 1.5 kg/m^2 per hour, the solar efficiency was determined to be 63.9 %. With time, the contact angle dropped from 78° to 9.65° . The fact that this type of membrane could be reused 20 times after usage was its best quality. This membrane is useful for solar steam generation since it is inexpensive and has high solar efficiency.[8]

Using polyurethane foam and filter paper combined with zinc carbide, a solar device was created. The device demonstrated good stability, foldability, and hydrophobicity. The device displayed a water evaporation flux of $1.43 \text{ kg/m}^2 \text{ hr}$ and a solar efficiency of 96 % at a mass loading of 85%. Ion concentration in the evaporated water was far lower than that recommended by the WHO for drinking water. One disadvantage is that the deposition vanishes from the sediment and must be redeposited for the duration of the night, a process known as self-recovery in this procedure. Water will smell bad and the device capacity to be recovered will be reduced if the salinity in the device rises by more than 15 %. The future of metal carbides in plasmonic applications is bright.[9]

Ti₃C₂T_x MXene nanoflakes were used to make a solar evaporator, and CIS NP was uniformly applied to its surface. The interlayer spacing increases as a result of the inclusion of NP, which enhances Maxine wettability and causes it to absorb more solar light. The hierarchal nanostructures seen in these nanoflakes aid in rapid water movement. This device displays water evaporation of 1.434 kg/m^2 every hour at 90 % solar efficiency for a cost of 62.35 gram per dollar.[10]

An interfacial solar evaporator was easily constructed in order to convert solar light into thermal energy. Fe_2O_3 nanoparticles were applied to a facial sponge that had a rough surface, omnidirectional solar absorption, and the ability to concentrate light on the membrane surface. With solar efficiency of 95 %, a water flux of 1.52 kg/m^2 per hour was observed. The membrane displayed a water flux of 33.84 kg/m^2 for 8.3 hours under two suns. The rejection of the orange dye also occurred, as demonstrated by Raman spectroscopy. Large-scale production is achievable since the fabrication is scalable.[11]

The researchers made Co-based MOFs that, after carbonization, act as carbon nanoplates and carbon nanoparticles that can collect solar energy and transform it into photothermal heat. The wood aerogel employed in this method is the supporting substance that made it possible for the device to float on its own. With a power density of 1 sun, the evaporator displayed a water flux of 1.52 kg/m^2 per hour and an evaporation efficiency of 92.42 %. For the whole 10 cycles, the evaporator displays the same amount of evaporation. It is seen that salt buildup has high resistance. The high evaporation and consistency demonstrated excellent possibilities for using solar energy to produce clean water.[12]

Black gold nanoparticles were applied to a sponge evaporator. The device's ability to withstand salt, which improves water evaporation efficiency over the course of prolonged operation, is one of its best qualities. The water flux was calculated to be 12.74 kg/m^2 per hour for 11 hours with a solar efficiency of 90 % under 10 kW/m^2 . It displays an hourly evaporation rate of 1.24 kg/m^2 under solar radiation 1. Through the capillary and gravitational forces of the melamin resin sponges, concentrated and freshwater are transported. This device maintained 80 % outdoor efficiency.[13]

Single-step pulsed laser deposition is used to synthesize a 2D layered alloy material that exhibits strong interactions between light and matter because of the abundance of intermediate band states in the material. The gadget in question is BiInSe₃@CF, and it shows a high rate of evaporation of 1.1 kg m⁻² h⁻¹ when exposed to solar radiation. Localized heating and phonon-assisted decay are the causes of the heating. Four orders of magnitude less ions were present in salty water, which resulted in a drop in ion concentration. Over the course of the 15 cycles, the device maintained its performance. This is all the result of localized decay by phonon assistance.[14]

The desalination procedure in this study uses a bioinspired surface solar heating mechanism. The various Au concentrations were used to prepare the plasmonic membranes. The membrane micropores assisted in the transmission of the water. The solar efficiency measured at 10 kW/m² came out to be 85 %. Because of the high plasmon dissipation and rapid transport of water in the microchannels, the membrane demonstrated solar absorption of up to 90 %. The membrane performed well in terms of producing clean water. The plasmonic membranes provide a water evaporation flux of 0.87 kg/m² hour upon 1 solar radiation and call for an expensive metal like gold. On the membrane, various gold concentrations were also examined.[15]

In another study, a membrane modified with nanoparticles was formed for the conversion of solar energy to heat energy. The prepared core-shell Ag@TiO₂ nanoparticles displayed self-floating behaviour and exhibited a higher absorbance. Under one sun's irradiation, the nanoparticles demonstrated a water flux of 1 kg/m² hour with a solar efficiency of 69 %.[16]

In this study, a 3D porous membrane made of aluminium that contains self-assembled aluminium nanoparticles was synthesized. The membrane served as a plasmonic absorber and floated on the water's surface. The membrane's solar efficiency was 90 % and its solar absorption was 96 %.

Under diverse settings, the membrane stayed stable for 25 cycles. The produced membrane was cost effective, had a significant plasmonic impact and was abundant in nature.[17]

Since solar energy is the most plentiful and readily available source, researchers in the study produced highly plasmonic functionalized materials made of cotton for water desalination using solar energy. Strong solar absorption was displayed by the metallic nanoparticles made of gold and silver, which then heated the environment. Cotton offered a hydrophobic surface that allowed absorbed materials to float on the water's surface and offered direct solar interaction with the materials there. This material E_w was determined to be $1.4 \text{ kg/m}^2 \text{ hr}$ under a single solar radiation and $11.3 \text{ kg/m}^2 \text{ hr}$ under eight solar radiations, respectively. Under both acidic and basic environments, the material demonstrated sustainability for the same rate of evaporation for the 10 cycles.[18]

In this study, the scientists have synthesized an evaporative device made of microporous membrane and plasmonic indium nanoparticles. The indium nanoparticles displayed a stronger plasmonic impact in comparison to the gold, silver, and aluminium nanoparticles, and the membrane's lightweight and porous structure allowed it to absorb light. The device effectively desalinated actual saltwater while floating on the water's surface. Throughout numerous cycles, the device remained stable. People in undeveloped places can utilise it easily because it is portable.[19]

Using 3D printing and drop casting, molybdenum disulfide layers were added to polyurethane sponges. These sponges demonstrated excellent photothermal characteristics, including rapid temperature rise of the surface water and accelerated evaporation. They also displayed hydrophobicity. These sponges had the ability to extract crude oil and perform the desalination process. The high evaporation rate (i.e., $3.5 \text{ kg/m}^2 \text{ hr}$) of these sponges is more than that of plain

MoS₂ and without sponges, respectively. These opened a brand-new route for the many environmentally friendly technology fields.[20]

The researchers presented a potential environmentally friendly and long-lasting approach for producing fresh water by solar-driven water evaporation. On the PTFE membrane, non-stoichiometric Co_{2.67}S₄ nanoparticles were deposited. The membrane demonstrated outstanding durability. Under two sun irradiation and a water flux of 2.62 kg/m² hr, the solar efficiency was 82 %. Additionally, bacterial cell walls were destroyed and their ability to multiply was hindered by photothermal heat conversion. These outcomes demonstrated the significant potential of the Final PTFE membrane for water filtration and photothermal water evaporation.[21]

In research, the researchers showed how Ti₂O₃ nanoparticles can be used as a photothermal medium for the seawater desalination process since they have a small band gap. The created Ti₂O₃ displayed absorption across the entire solar spectrum. The surface area for absorption was boosted by the small dimensions of nanoparticles. With a solar efficiency of 92.5 %, this material has an evaporation flux of 1.35 kg/m² hr. Thermal catalysis and photothermal treatment are further applications for this material.[22]

A study used synthesized polyacrylonitrile nonwoven fabrics to solve the problem of salt buildup in nanostructure membranes. These were produced using a basic electrospinning technique. The synthesized substance displayed a 90.8% light absorption efficiency. Under one sun, the evaporation rate was found to be 1.44 kg/m² hr. The accumulated salt can be removed easily from the fabric by washing it after the desalination procedure. This approach can also be used for large-scale production.[23]

The capacitive deionization procedure has been employed in this study to address the global water crisis. The interlayer expansion technique can increase desalination by 30 %. In this case, rGO-CNT aerogel contained WS₂ nanoflowers as an anode. 1.62 kg/m² per hour of water flux was calculated with an 83 % solar efficiency.[24]

In another study, the distillation membrane surfaces had CNTs immobilized there. Due to the presence of CNTs on the hydrophobic membrane pores, they alter the interactions between water and membrane. And they stop fluids from entering the membrane pores. Because of this setup, the water flux rose up to 1.85 kg/m² hr, and the 34000 ppm salt content was reduced.[25]

In a study, the researchers developed a flexible Janus membrane-based evaporation method. The membrane was constructed of a silica membrane with embedded hybrid GO/CNTs, allowing the hybrid structure to localise heat while the membrane could pump water. Different outcomes were produced by altering the membrane's shape and thickness. With a solar efficiency of 74 % and an evaporation rate of 1.30 kg/m² hr under one solar irradiation, the membrane's ability to self-clean and maintain stability demonstrated its enormous potential for solar desalination.[26]

The delamination of GO in a study presents a practical barrier for solar desalination. By self-linking the polyionic liquid, GO stability was increased without affecting the hydrophilic structure of the molecule. Additionally, CNT was added, increasing stability even between pH 1 and 13. Under one sun, a high evaporation rate of 1.87 kg/m² hr was attained and stayed constant for 14 hours. This has a daily output of 10.1 kg/m² water, enough for 5 adults.[27]

For solar steam generation devices, a modified CNT with a wood matrix was synthesized in another research. Microchannels in the wood matrix allowed the water to be pumped uphill. These

devices demonstrated strong solar light absorption, low heat conductivity, and low price. A water evaporation flux of $0.95 \text{ kg/m}^2 \text{ hr}$ was reported with an efficiency of 81 % at 10 kW cm^{-2} . [28]

Researchers created a plasmonic wood with nanoparticle decorations that has microporous and nonporous channels for the quick transfer of water. Pd, Ag, and Au nanoparticles have been deposited on the membrane. With the help of the five solar radiations, the plasmonic displayed solar absorption in the 200–2500 nm region. A result of above 99 % for absorption is very good, $1.0 \text{ kg/m}^2 \text{ hr}$ water flux with 85 % sun efficiency. For 144 hours, the product was recyclable and self-cleaning. These types of wood provided the desalination process with more options. [29]

A stand-alone device for the desalination of seawater using photothermal heat conversion was developed. A single component of a graphene structure that resembled a 3D honeycomb made up the converter. This machine has a high conversion efficiency and low cost for turning water from various sources into steam. This device had a solar efficiency of 87% and a water flux of 2.6 kg/m^2 per hour. Drinkable water may be produced with this system from both seawater and sewage water. [30]

In research, scientists created an independent hydrothermal membrane for solar steam production and fog collecting. The membrane was made up of three-dimensional microstructures that offered a large surface area for the conversion of solar energy to heat. Under one solar radiation, the value of water flux was 3.64 kg/m^2 per hour. This hydrothermal membrane can produce 34 L m^{-2} of fresh water. The microstructures were like 3D trees and were produced using 3D printing. [31]

MWCNTs were doped into the rGO layers to form a 2D rGo and 1D MWCNTs membrane. These photothermal membranes are wettable, lose structure, and have regulated microstructure. These were submerged in the PVDF for longer and attained a sun efficiency of 84.5 % when exposed to

one solar ray. Compared to the pure chemicals, these findings were better. The water flux through this membrane stayed within the range of 1.19 to 1.31 kg m⁻² per hour.[32]

In another study, membranes made of vertically oriented graphene sheets were synthesized using the antifreeze-assisted freezing method. The VA-GSM promoted the movement of water through the channels and provided excellent light absorption for the conversion of solar energy to heat. With an efficiency of 86.5 % and 94.2 %, the water flux under one sun was 1.62 kg m⁻² hr⁻¹ and 6.25 kg m⁻² h⁻¹ under four suns. The manufactured material membranes for desalination were superior to the carbon material membranes that had previously been described.[33]

The GCP membrane was made by crosslinking PIL and nearby GO nanosheets under moderate circumstances. These had great hydrophilicity, outstanding stability, and an evaporation rate of 1.87 kg/m² h under one sun. They also performed well in both basic and acidic water environments. Further research revealed that on bright days, the GCP membranes produced 10.1 kg m⁻² and on cloudy days, 5.1 kg m⁻². Therefore, solar steam generation and desalination are both possible with this method.[34]

In a study, a photothermal aerogel was created by mixing agarose, cotton, and a CuS yolk-shell nanocage. The water flux across this membrane was 1.63 kg/m². A 94.9 % solar efficiency was observed. On a vast scale, photothermal aerogel can be made. The membrane held steady for 15 cycles in a row. The sole value observed for the ion concentration was 0.54 mg L⁻¹. There is a lot of potential for practical use of this information.[35]

Bamboo charcoal was employed in another study to generate interfacial solar steam. The porous structure of Bamboo charcoal allowed for localised heating and full spectrum solar absorption.

Under the influence of one sun, the solar efficiency measured to be 84 %. It can therefore supply fresh water. It is long-term stable, affordable, and sustainable.[36]

A photothermal AuNPs@g-C₃N₄/CMF (AMF) membrane for solar water purification was produced by combining AuNPs@g-C₃N₄ with carbonized melamine foam (CMF). By adding a dicyandiamide mediator, the as-prepared AuNPs@g-C₃N₄ were simply distributed on the top surface of the AMF membrane in order to increase the photothermal conversion efficiency and lower the cost of the AMF membrane. Through this procedure, the top surface of the CMF was uniformly coated with AuNPs, which can increase light absorption. In contrast, the bottom surface of the CMF, which was not coated with AuNPs, has a reasonable level of thermal insulation performance. The intriguing double-layer heterostructure helps the AMF membrane attain a high evaporation rate (1.675 kg m⁻² h⁻¹) and photothermal efficiency (94.03 %). The AMF membrane demonstrated superior desalination performance.[37]

Using a hydrophilic nylon filter membrane and hydrophobic bamboo-structured nitrogen-doped carbon nanotubes (Co@C/NCNT), a novel Janus Co@C/NCNT photothermal membrane with asymmetric surface wettability and multiple optical absorption pathways was synthesized. Under a single sun irradiation, the Janus Co@C/NCNT-based solar evaporator achieves a high water evaporation rate of 1.55 kg m⁻² h⁻¹ and a photothermal conversion efficiency of 89.7 %. Additionally, the Janus evaporator's design is practical and adaptable, allowing it to clean a variety of high-concentration wastewater, including that containing organic dyes, heavy metals, and harsh, highly acidic, or alkaline solutions reliably and successfully.[38]

A straightforward method was employed for creating core-sheath polyacrylonitrile nanofibers with PPy coating (PAN@PPy NFs). The random porosity features of the composite provided direct, hydrophilic pathways for better water transfer through the wicking effect. Additionally, a

significant increase in light-trapping efficiency leads to a significant decrease in transmittance and reflection over a wide spectral range. With a solar steam conversion efficiency of up to 83.5 %, this design achieves a high water evaporation rate of 1.633 kg/m² h. Additionally, the composite shows a lot of potential for solar-driven desalination due to its cost-effectiveness, scalability, and exceptional durability.[39]

3. Experimental

3.1 Materials Required for Synthesis:

The chemical reagents utilized in the synthesis of molybdenum selenide, Ni-doped molybdenum selenide, and Co-doped molybdenum selenide included selenium powder, sodium molybdate dihydrate, hydrazine hydrate, nickel chloride hexahydrate, and cobalt chloride hexahydrate. The solvent chosen for the entire synthesis process was water due to its universal solvent property, availability, and non-toxic nature."

3.2 Synthesis of Molybdenum Selenide:

The synthesis started with 20 mL of water containing 0.32 g of $\text{Na}_2\text{MoO}_4 \cdot 2\text{H}_2\text{O}$ (0.04 M). This mixture was vigorously stirred for 15 minutes to ensure complete dissolution of sodium molybdate dihydrate. Then, 0.12 g of Se (0.04 M) powder was dissolved in 10 mL of hydrazine hydrate ($\text{N}_2\text{H}_4 \cdot x\text{H}_2\text{O}$). This solution was added dropwise to the aforementioned stirring solution, resulting in the formation of a black precipitate indicating the formation of Molybdenum Selenide. The resultant mixture was transferred to a Teflon lined autoclave (50 mL) and heated at 180 °C for 12 hours in an oven. Upon completion of the hydrothermal reaction, the autoclave was allowed to cool to room temperature. The black precipitates formed were then collected, washed with water and ethanol to remove impurities, and dried overnight in a vacuum oven at 45 °C.

Synthesis of MoSe₂ by Hydrothermal Method

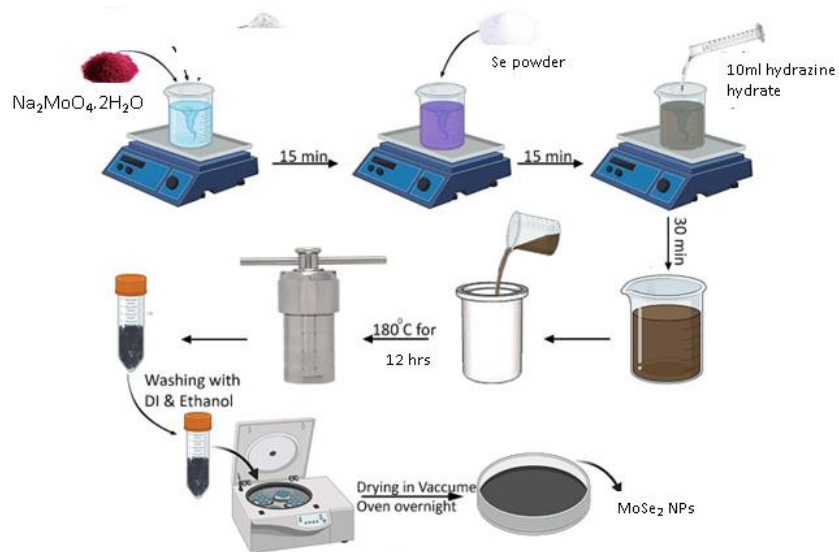


Figure 5: MoSe₂ Synthetic Scheme

3.3 Synthesis of Nickel-Doped Molybdenum Selenide:

For the synthesis of Nickel-doped Molybdenum Selenide, 0.16 g of Na₂MoO₄·2H₂O (0.02 M) and 0.20 g of NiCl₂·6H₂O (0.02 M) were mixed in 20 mL of water. This solution was stirred vigorously for 15 minutes, ensuring complete mixing of the components. Then, 0.12 g of Selenium (0.04 M) powder dissolved in 10 mL of hydrazine hydrate (N₂H₄·xH₂O) was slowly added. The black precipitate observed indicated the successful formation of Ni-doped Molybdenum Selenide. This mixture was then transferred into a Teflon lined autoclave (50 mL), heated at 180 °C for 12 hours, and allowed to cool down to room temperature. The final precipitate was collected, washed with water and ethanol, and dried overnight in a vacuum oven at 45 °C.

Synthesis of NiMoSe₂ by Hydrothermal Method

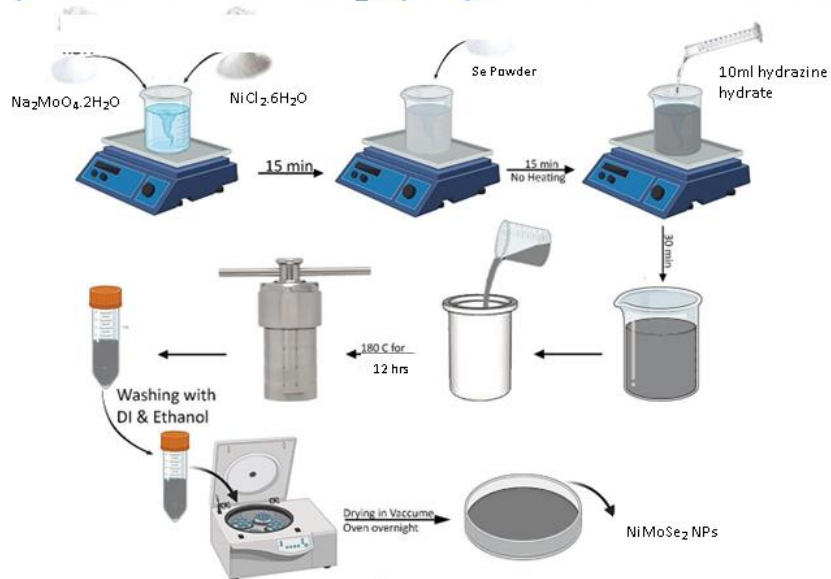


Figure 6: NiMoSe₂ Synthetic Scheme

3.4 Synthesis of Cobalt-Doped Molybdenum Selenide:

The procedure for the synthesis of Cobalt-doped Molybdenum Selenide was similar to that of Ni-doped Molybdenum Selenide. Initially, 0.16 g of Na₂MoO₄·2H₂O (0.02 M) and 0.20 g of CoCl₂·6H₂O (0.02 M) were mixed in 20 mL of water and stirred for 15 minutes. A solution of 0.12 g of Selenium (0.04 M) powder in 10 mL of hydrazine hydrate (N₂H₄·xH₂O) was then slowly added, which led to the formation of a black precipitate, indicative of successful synthesis. This was transferred into a Teflon-lined autoclave (50 mL), subjected to heating at 180 °C for 12 hours, and allowed to cool at room temperature. The final black precipitate was collected, washed with water and ethanol, and then dried overnight in a vacuum oven at 45 °C.[40]

Synthesis of CoMoSe₂ by Hydrothermal Method

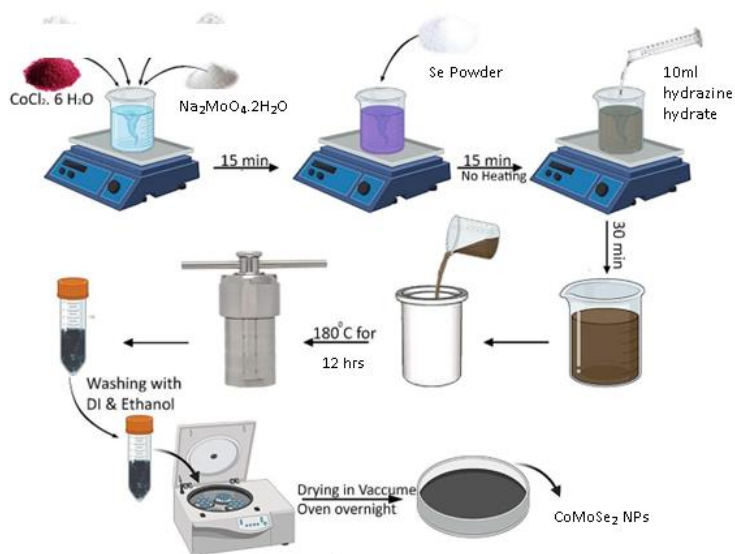


Figure 7: CoMoSe₂ Synthetic Scheme

3.5 Preparation of Nanoparticle-Embedded Cotton Gauze Membranes:

This part involved the preparation of nanoparticle-embedded cotton gauze (CG) membranes using a solvothermal method. The nanoparticles of MoSe₂, NiMoSe₂, and CoMoSe₂ were uniformly deposited on the CG. This was achieved by creating an ethanol-based slurry containing these nanoparticles.

The slurry was then subjected to sonication for an hour at a temperature of 30 °C. Sonication was applied to ensure a uniform distribution of nanoparticles within the slurry, thus leading to a more effective deposition on the CG membrane.

The CG used in this process was sourced from a local shop. It was selected due to several of its desirable properties. Specifically, it has low thermal conductivity, is lightweight, affordable, and exhibits excellent stability. Its thermal conductivity, an essential factor in this application, was in the range of 0.02 W/m K.

For the purpose of consistency across all experiments, the CG was meticulously cut to identical dimensions. This step ensured that any variability in results could be attributed to the experimental conditions rather than differences in the size of the CG membranes.

After sonication, the nanoparticle-coated CG membranes, now referred to as MoSe₂@CG, CoMoSe₂@GC, and NiMoSe₂@GC, were left to dry naturally in an open-air environment. This ensured the complete evaporation of the residual ethanol and resulted in the firm attachment of nanoparticles onto the CG.

Finally, to augment the floatability of the device on the water surface – a crucial aspect for solar-driven desalination – an additional lining of polyethylene was applied. Polyethylene, due to its buoyant nature, provided enhanced floatability to the nanoparticle-embedded CG membranes, making them more efficient for practical application.

Our design strategy depends on the successful adhesion of nanoparticles onto the cotton gauze (CG). Given that CG is inherently hydrophobic, it has the capability to float on the seawater's surface, while simultaneously supporting the weight of the nanoparticles. This is facilitated by the strategic application of polyethylene lining on the membrane's edges.

Interestingly, the nanoparticles integrated onto this membrane demonstrate hydrophilic properties. Their surface-floating behaviour enables efficient photothermal energy conversion, which is central to the desalination process.

The implementation of this device is further amplified by the porous nature of the membrane, which not only increases the interaction surface area but also facilitates easy water transportation from underneath to the surface. The low thermal conductivity of the membrane induces a

temperature disparity between the bulk water and the surface water where the membrane is deployed.

Such a setup allows for the easy synthesis and embedding of nanoparticles onto the membrane, enabling the occurrence of surface phenomena without interfering with the water body beneath. Salts are effectively trapped on the membrane surface, and the high-water flux contributes to increased water evaporation. The system design eliminates the risk of water fouling or scaling, maintaining an efficient operation over time.

The simplicity and cost-effectiveness of the hydrothermal method used to synthesize the nanoparticles, coupled with their stability, further enhance the viability of this solar-driven desalination strategy.

3.6 Indoor Desalination Experiment

Following the preparation of the nanoparticle-embedded membrane, the indoor desalination experiment was initiated. This involved placing the fabricated membrane on the surface of a beaker filled with a simulated seawater solution, specifically 30 ml in volume.

The experiment was conducted under artificial illumination provided by a Xenon Lamp Power Supply XPS -300TM. This high-intensity light source was chosen for its ability to reproduce the ultraviolet-visible light spectrum similar to that of natural sunlight.

We measured the mass change of the desalinating device at ten-minute intervals using a high-precision METTLER TOLEDO electronic balance. This systematic recording of mass change was key in determining the evaporation rate and, subsequently, the desalination performance of the membrane.

Concurrently, we monitored the fluctuation in surface temperature with the assistance of an IR imaging camera. This thermal monitoring provided insights into the photothermal energy conversion and its correlation with the desalination efficiency.

To ensure a constant and standardized irradiation on the desalinating device, we employed a handheld solar power meter. This instrument allowed us to accurately regulate and maintain the solar intensity during the course of the experiment.

The evaporated water produced in this process was then carefully collected. Its ion concentration was analysed, providing crucial data on the quality and potability of the desalinated water. The data from these measurements were vital in assessing the effectiveness and efficiency of our nanoparticle-embedded membrane in the desalination of seawater.

3.7 Outdoor Desalination Experiment

To evaluate the performance of the nanoparticle-embedded membrane under real-world conditions, an outdoor desalination experiment was also done. This experiment took place on the grounds of the SNS Department in NUST Islamabad. A time window from 12 pm to 2 pm was selected to take advantage of the highest sunlight intensity during the day.

As in the indoor experiment, we monitored the mass change of the desalinating device at ten-minute intervals. We utilized the same METTLER TOLEDO electronic balance for consistency and to enable direct comparison between the indoor and outdoor experimental results.

The intensity of sunlight was continuously tracked using a solar power meter. This allowed us to correlate the solar intensity with the desalination performance of the nanoparticle-embedded membrane.

For the outdoor experiment, we positioned the evaporating device directly under the natural sunlight. It was placed on a 50 ml beaker that was filled with 30 ml of simulated seawater. This setup mimicked the natural environment where the device would typically operate, providing us with practical insights into the device's performance and potential for real-world application. The resulting evaporated water was carefully collected for subsequent analysis of its ion concentration.

3.8 Indoor Experiments in Absence of Light

To gain a comprehensive understanding of the impact of solar light on the desalination process, we also performed a set of experiments in a darkened laboratory environment. This effectively isolated the effect of photothermal energy conversion and allowed us to observe the behavior of the membrane under conditions devoid of any sunlight.

Much like the previous experiments, we maintained a strict routine of monitoring the mass change at every ten-minute interval. Our trusted METTLER TOLEDO electronic balance served in the measurement of these alterations, ensuring consistency across all experimental conditions.

Interestingly, a marked difference in the temperature fluctuations of the desalinating device in the absence of solar light was noted. This difference reaffirmed the critical role of sunlight in the photothermal conversion and subsequent desalination performance of the nanoparticle-embedded membrane. The observations gleaned from this lightless experiment helped to highlight the importance and efficiency of solar energy in driving the desalination process.

4. Results and Discussion

4.1 Material characterization of all the prepared MoSe₂, NiMoSe₂ and CoMoSe₂

The crystalline structure of the prepared samples was analyzed by X-ray diffraction analysis.

Figure 4.1 shows the XRD pattern of the obtained MoSe₂, NiMoSe₂ and CoMoSe₂. These were matched with the already reported literature. The diffraction peaks observed at the angles of 31.9° and 56.5° correspond to (100), and (110) planes of MoSe₂ showing that it has a highly amorphous structure. The diffraction peaks observed at the angles of 11.38°, 27.65°, 33.66°, 45.17°, 51.20°, 56.90° and 63.90° correspond to (002), (100), (120), (105), (002), (008) and (122) planes of CoMoSe₂. The diffraction peaks observed at the angles of 33.70°, 38.10°, 45.00°, 50.64°, 55.03°, 60.05° and 61.94° correspond to (110), (002), (102), (110), (200), (103) and (201) planes of NiMoSe₂ showing that it has a highly crystalline structure.

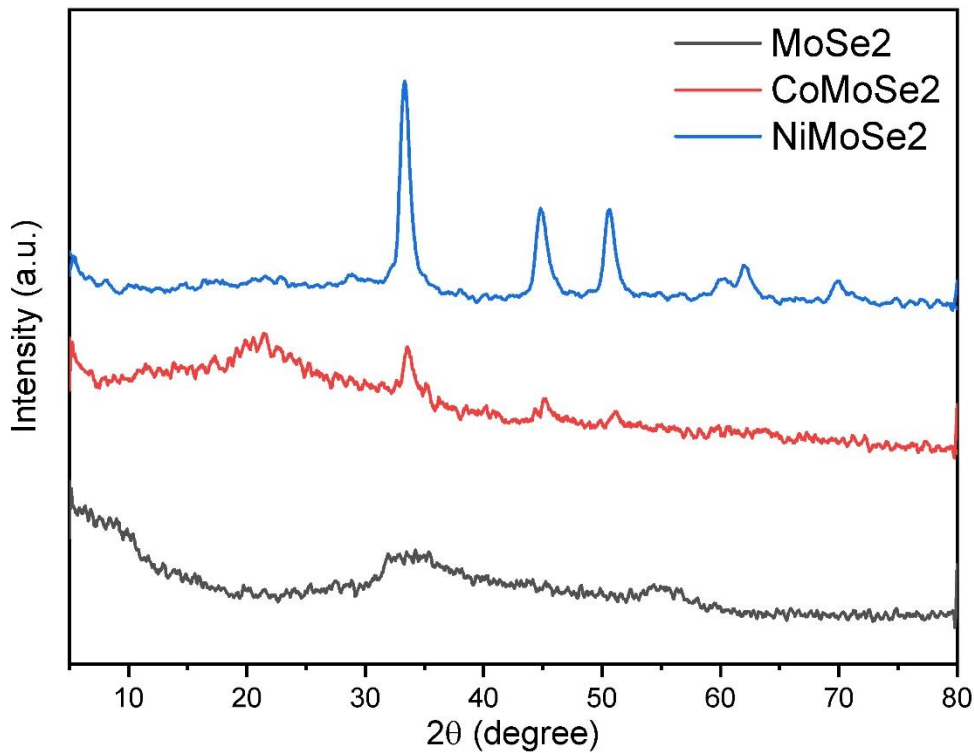


Figure 8: XRD Spectra Of MoSe₂, CoMoSe₂ and NiMoSe₂

$$D = \frac{k\lambda}{\beta \cos \theta}$$

Equation 4: Debye Scherrer Equation

In this equation the k is the factor of shape, Theta can be the diffraction angle and β is the half maximum of the line at full width. The average crystallite sizes of these samples are as follows.

Table 1

Sample	Crystallite Size (nm)
MoSe ₂	15.75
CoMoSe ₂	11.41
NiMoSe ₂	6.79

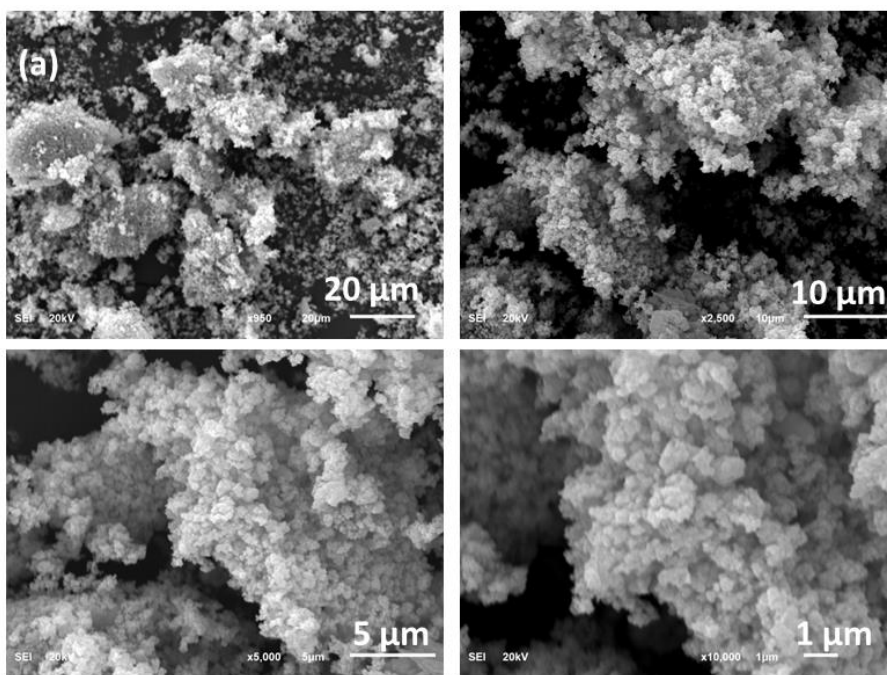
The SEM images are used to investigate the morphologies of the synthesized MoSe₂ nanoparticles and also of the NiMoSe₂ and CoMoSe₂ nanoparticles. The average particle size is also calculated by using these images. As we can see the MoSe₂ morphology as flower like particles which are coagulating and increasing the surface roughness. When the SEM images of CoMoSe₂ were analyzed, the coral-like morphology was observed with smoothness to some extent. The SEM images of NiMoSe₂ showed the hexagonal geometry of the respective nanomaterial with a high degree of crystallinity.

EDS analyses of all the samples were also carried out in order to confirm the presence of respective elements in the prepared materials. Mo and Se are present which confirms the successful synthesis of the material. Further, the Elemental mapping was also carried out which indicates the presence of both elements on the same location and confirms the MoSe₂ synthesis. The EDS analysis of CoMoSe₂ and NiMoSe₂ was also done to confirm the presence of the elements in the respective

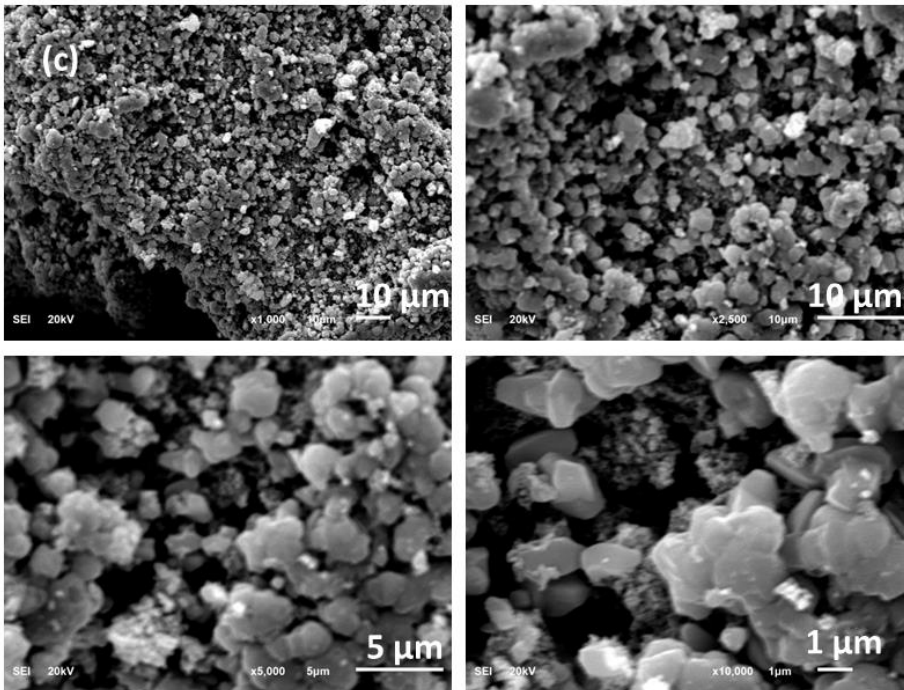
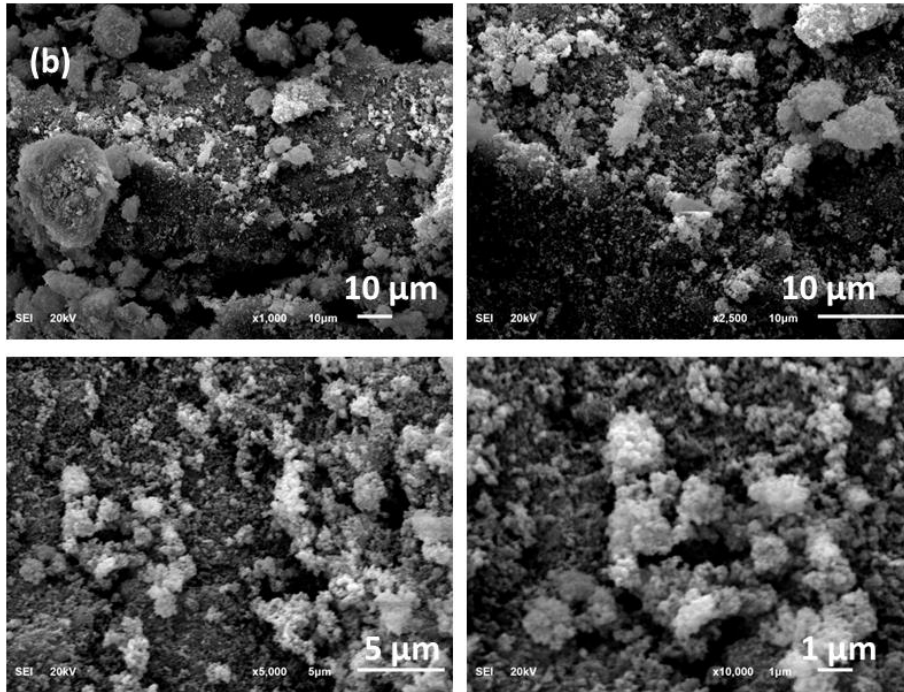
samples. The presence of all the 3 components is seen in the EDS spectrum and the elemental mapping was also done for the confirmation of elements.

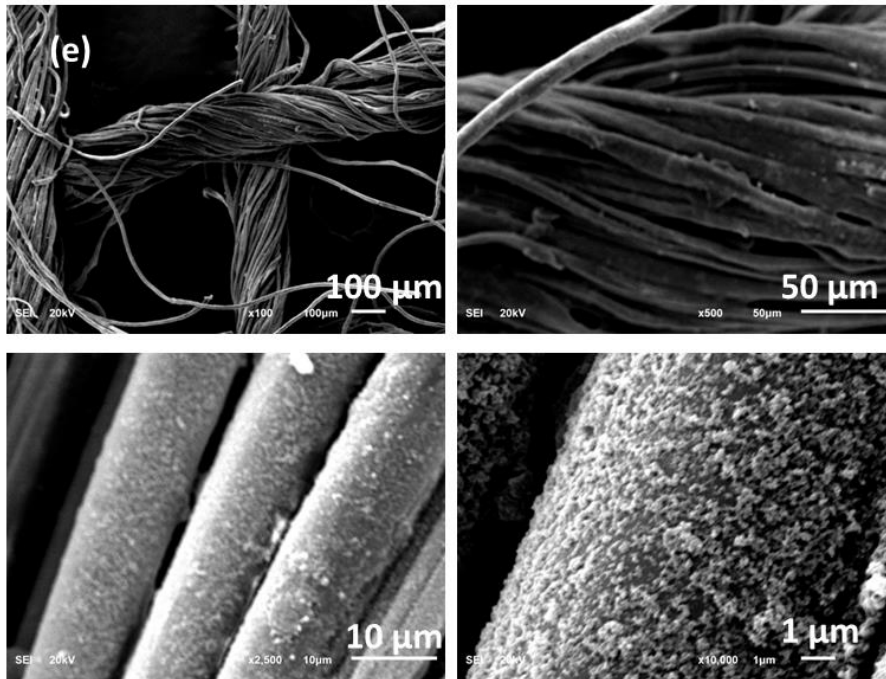
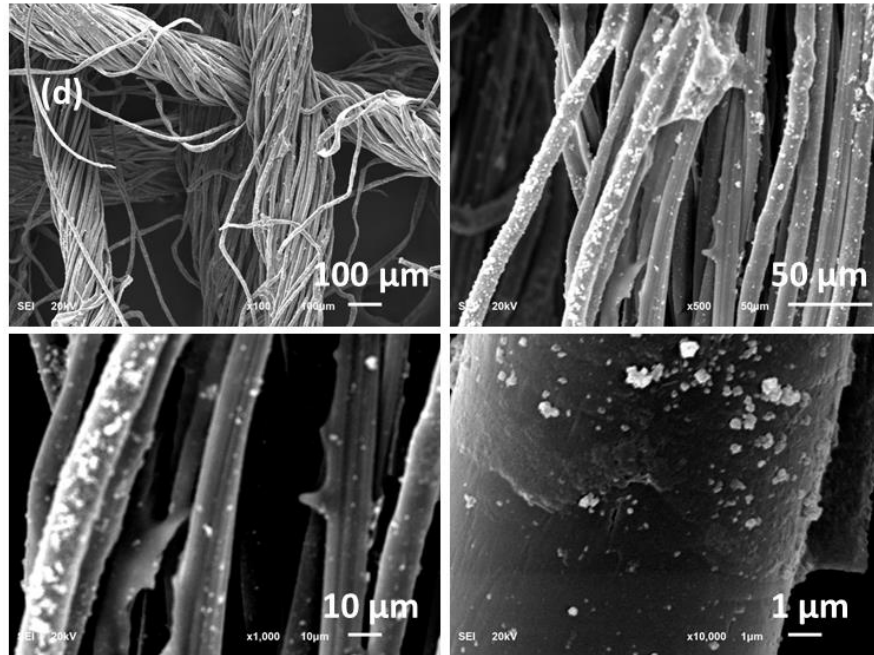
The prepared materials were deposited on cotton gauze which was used as substrate. The SEM images were taken in order to reveal the morphology of the adsorbed materials on the cotton gauze. As we can see in the figures that the particles are deposited on the cotton fibers which confirms the presence of the synthesized material on the cotton gauze.

EDS of the prepared materials on the cotton gauze are determined which confirms the presence of all the 3 elements on the cotton gauze.



S





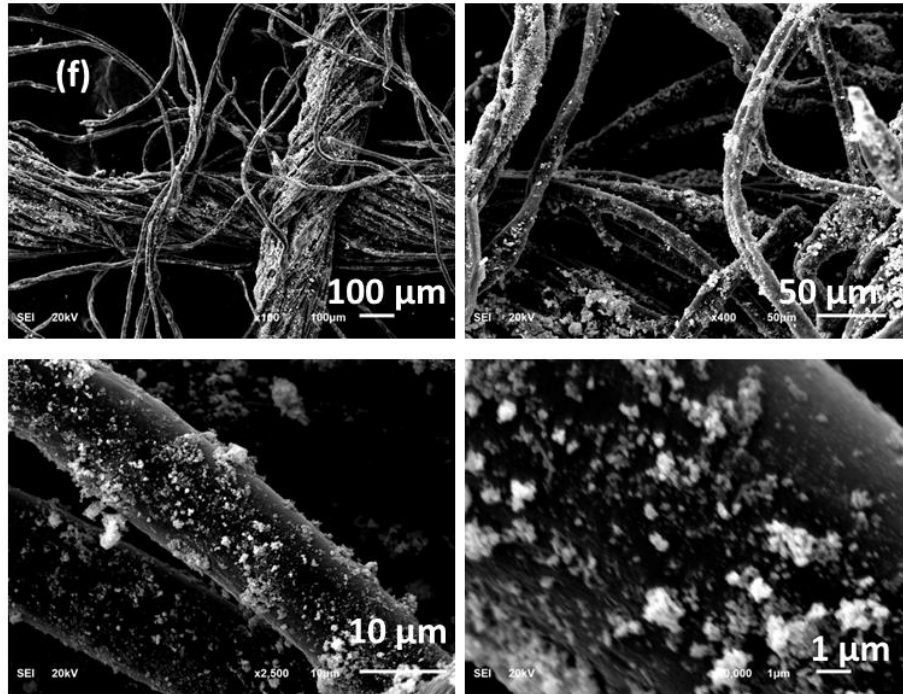


Figure 9: SEM images of (a) MoSe_2 , (b) CoMoSe_2 , (c) NiMoSe_2 , (d) $\text{MoSe}_2@\text{CG}$, (e) $\text{CoMoSe}_2@\text{CG}$ and (f) $\text{NiMoSe}_2@\text{CG}$

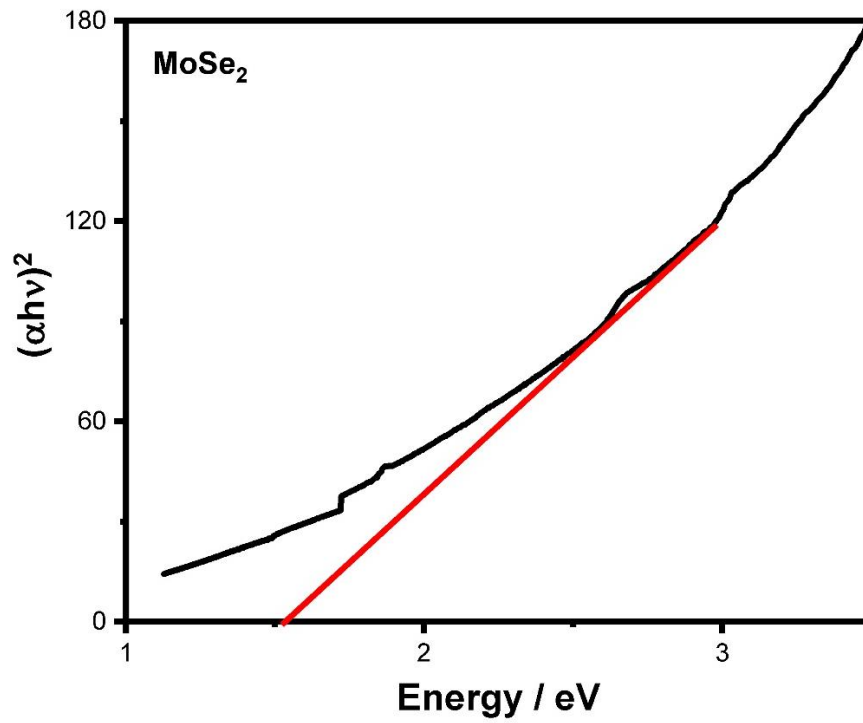


Figure 10: Tauc Plot of MoSe_2

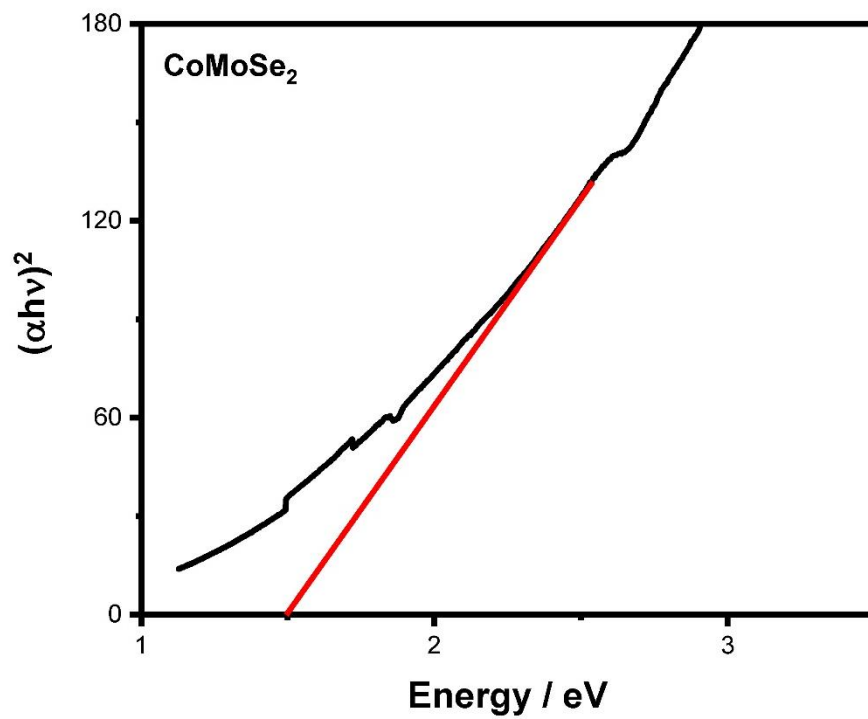


Figure 11: Tauc Plot of CoMoSe₂

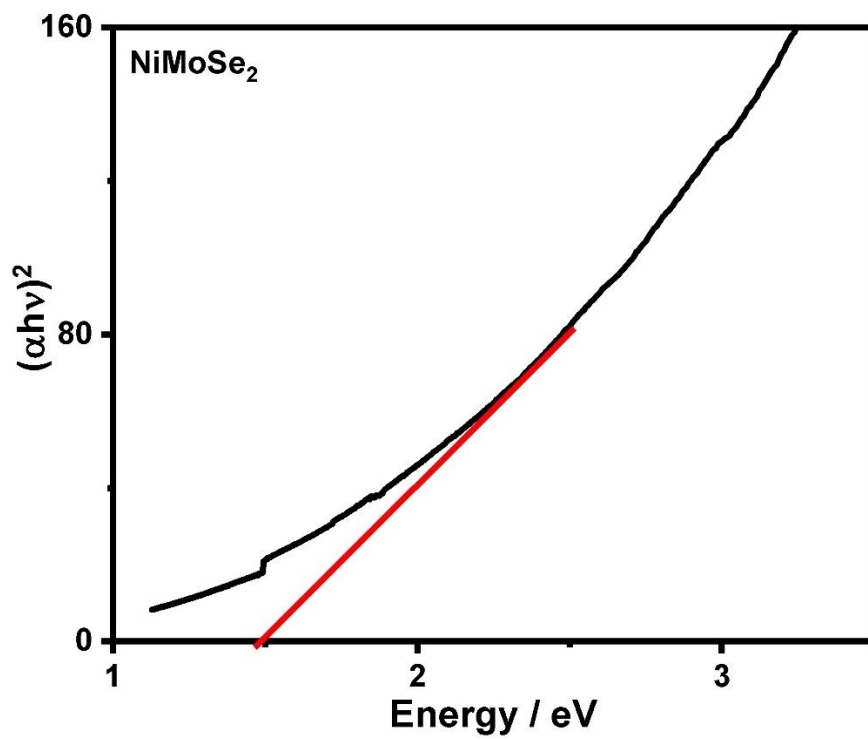


Figure 12: Tauc plot of NiMoSe₂

4.2 Mechanism of Plasmonic Resonance

The metal chalcogenides represent an interesting class of plasmonic materials which oscillates by the absorption of light. These semiconductor materials can easily localize the sunlight on their surface and this phenomenon can be enhanced by the doping effect. The mechanism of a highly efficient membrane can be unveiled. It consists of light absorbance, decay of photoexcited electrons and the interfacial heat release in the surrounding media.

According to the DRS absorbance graph, we can see that the synthesized material can absorb light in the UV-Visible range. When the light falls on the self-floating nanoparticles containing a membrane, heat is localized on the surface by these nanoparticles. LSPR effect is shown by these nanoparticles which depend upon the surface morphology and resonance frequency. The nanoparticles absorb the light, and the electrons are excited. As the energy levels are present in the forbidden region, the electrons can easily go to the conduction band as the band gap is also small. Due to which the electron scattering, and recombination process take place as e^- to e^- , e^- to photon and electron to phonon transfer can take place. In the first 100 fs, the electron-hole pairs scattering takes place and the electrons decay by the emission of photons or electron interaction takes place. The electron energy is redistributed by the hot carriers and through thermal conduction, the surrounding media is heated. This process can also be called plasmonic near-field enhancement.[41]

4.3 Evaporative and Photothermal Efficiencies of the Evaporating Device

Various types of membranes were designed to explore the evaporative performance, as indicated in the figure. The membranes were made using a simple process that involved dipping them into the slurry, sonication, and overnight drying at room temperature. These membranes can convey water in a two-dimensional (2D) manner, and expanded polyethylene was utilized to make them

stably float on the water surface. Each slurry included a specific amount of nanoparticle powder, and it was ensured that it remained adherent to it.

The membrane was placed in a 50 ml beaker that contained a 35000 ppm NaCl solution to simulate artificial seawater. Earlier experiments had been carried out using the same volumes of pure water. The gadget may float on the water surface, and the instant it made contact with the water, the membrane began to become wet. Because of the device porosity, the wetting began equally at each site. It only took a few seconds to complete this. This is a good evaporative technique because the device can evaporate the surface water without heating the water in bulk.

4.4 Contact Angle Measurement:

The water contact angles of samples with the substrate were also examined to determine the hydrophilicity of the nanoparticles. Cotton gauze is the substrate chosen for our experiment because of its beneficial qualities. The contact angle of the bare cotton gauze was determined. The contact angle of untreated cotton gauze, as depicted in figure (b), is 108.9° . This shows that the membrane is hydrophobic and can self-float. Due to the surface porosity and hydrophilicity of the produced material, as shown in the above figure, all samples showed the water contact angle of 0° when the material was adsorbed on the membrane.

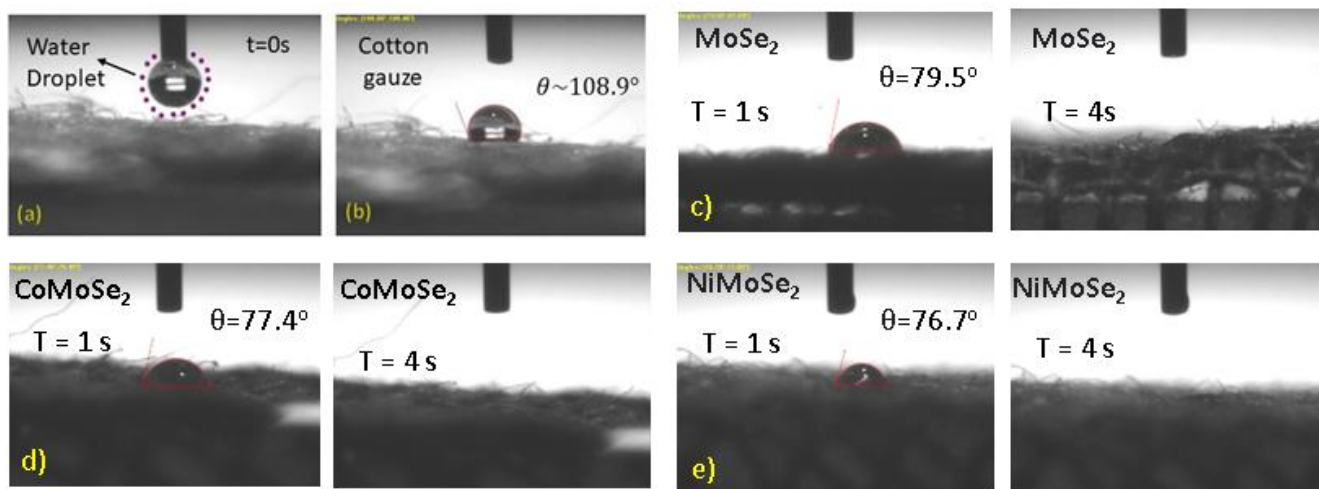


Figure 13: Water contact angles of (b) Cotton Gauze, (c) MoSe₂@CG, (d) CoMoSe₂@CG and (e) NiMoSe₂@CG

4.5 Photothermal Conversion Performance:

4.5.1 Evaporative Performance under one Solar Radiation:

For investigating the evaporative performances of MoSe₂@CG, CoMoSe₂@CG and NiMoSe₂@CG membranes, the mass change for the simulated seawater under solar radiation of 1 kW m⁻² was determined. The evaporative performances of different synthesized membranes were calculated using the formula as follows.

$$E_w = \frac{\Delta m}{A \cdot t}$$

The low thermal conductivity of cotton gauze attributes does not allow the dissipation of heat in the surrounding environment. The simulated seawater showed an evaporation flux of 0.46 kg m⁻² h⁻¹. The evaporation rate shown by MoSe₂@CG was 1.54 kg m⁻² h⁻¹, that shown by CoMoSe₂@CG was 1.85 kg m⁻² h⁻¹, and that shown by NiMoSe₂@CG was 2.52 kg m⁻² h⁻¹ which is the highest of all the samples prepared. So, by doing these experiments we have obtained the right material for the desalination of seawater using solar light.

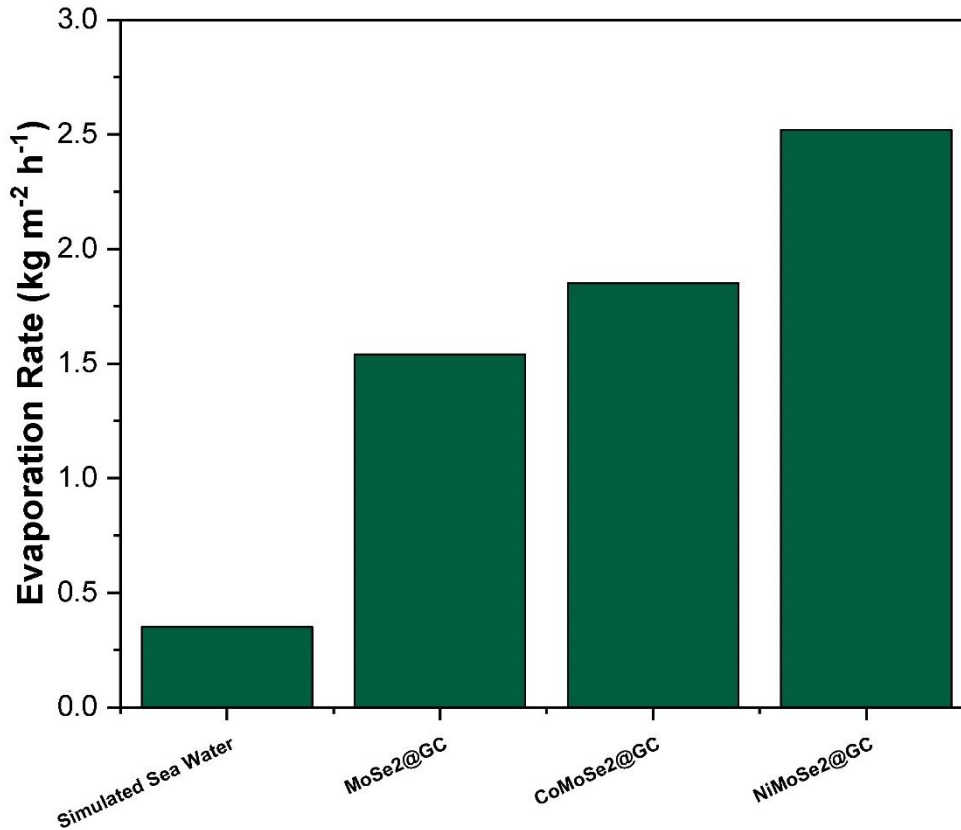


Figure 14: Evaporation Flux

4.5.2 Evaporative Performances at Room Conditions:

The membranes were then tested at room conditions by placing the beaker in the room and measuring the water flux by calculating the mass difference after an hour. The mass difference was calculated by the same weighing balance. The water flux of MoSe₂@CG was 0.46 kg m⁻²h⁻¹, that of CoMoSe₂@CG was 0.43 kg m⁻²h⁻¹, and that of NiMoSe₂@CG was 1.05 kg m⁻²h⁻¹.

4.6 Solar Efficiencies of the Materials:

The mass change of the evaporating apparatuses and the mass loss of saltwater in the dark can be subtracted to find the solar efficiency of a material, which can then only be found. The power of irradiation has an impact on solar efficiency as well, and in this work, 1 kW m⁻² solar power is used. The temperature of the substance that is being exposed to radiation affects the H_{LV}. The formula for calculating solar efficiency is as follows.

$$\eta = \frac{mh_{lv}}{C_{opt}q_i}$$

Here η represents Solar Efficiency. The difference between the mass loss of saltwater owing to solar light and the mass loss of seawater in the dark, is represented by m . The water flux in the sun light for our finest material is $2.52 \text{ kg m}^{-2} \text{ h}^{-1}$. The same substance as $\text{NiMoSe}_2@CG$ exhibits a water flux of $1.05 \text{ kg m}^{-2} \text{ h}^{-1}$ in complete darkness. The value of m that is employed in the equation is determined by the difference in the mass loss of these. At various temperatures, H_{LV} varies. The change in surface temperature from the start of light irradiation to the conclusion of the experiment is known as sensitive heat, or H_s . C_{opt} has the value of 1 and is called the spotlight multiple in this experiment. Power density, or q_i , is 1 kW m^{-2} . Unit conversions should be considered when determining solar efficiency. There is no unit for η . The solar efficiency calculations for the prepared materials are displayed in the table below.

Table 2

Sr. no.	Materials	Water flux with solar light $\text{kg m}^{-2}\text{h}^{-1}$	Water flux without solar light $\text{kg m}^{-2}\text{h}^{-1}$	H_{lv} kJ kg^{-1}	H_s kW	q_i kW m^{-2}	Solar efficiency %
1	MoSe_2	1.54	0.46	2408	5.9	1	72.3
2	CoMoSe_2	1.85	0.43	2408	7.7	1	92.6
3	NiMoSe_2	2.52	1.05	2409	9	1	94.9

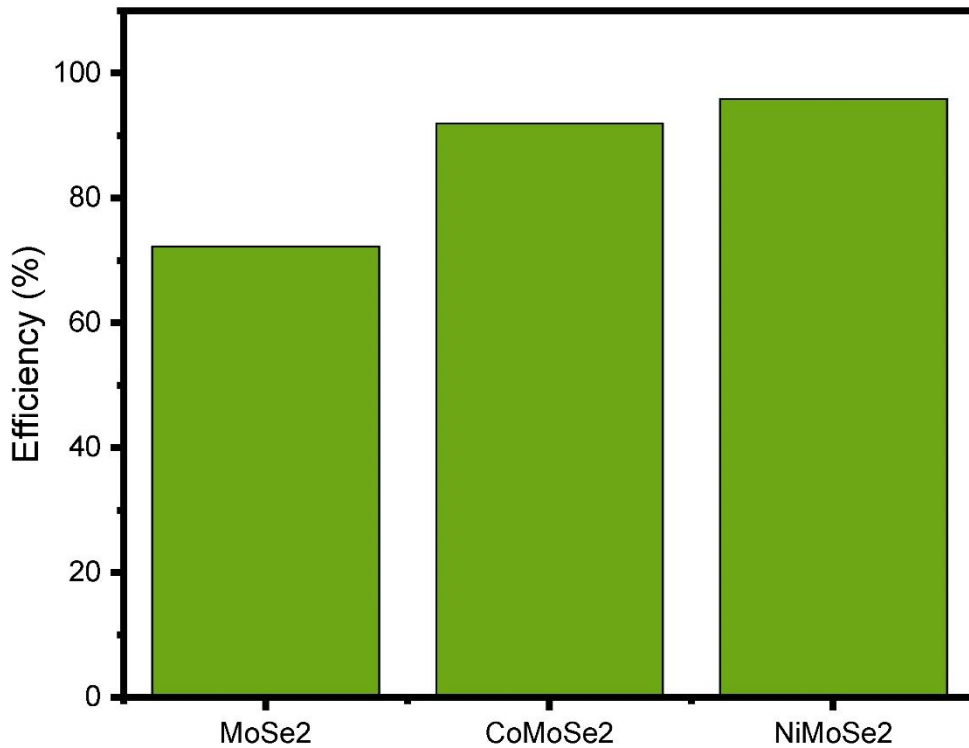


Figure 15: Solar Efficiencies

4.7 Photothermal Efficiencies measurement using IR imaging:

The surface temperatures of the membranes for desalination using solar light were measured using a thermal imaging camera. The portable thermal imaging camera measures the observed temperature differences. A temperature profile can be seen on the right side of the image, which was used to obtain the immediate thermal photographs. From 0 minutes to 60 minutes, thermal pictures were obtained every 5 minutes. A graph is drawn with time on the x-axis and the temperatures on the y-axis. The graph below is used to compare the photothermal efficiencies of all the membranes.

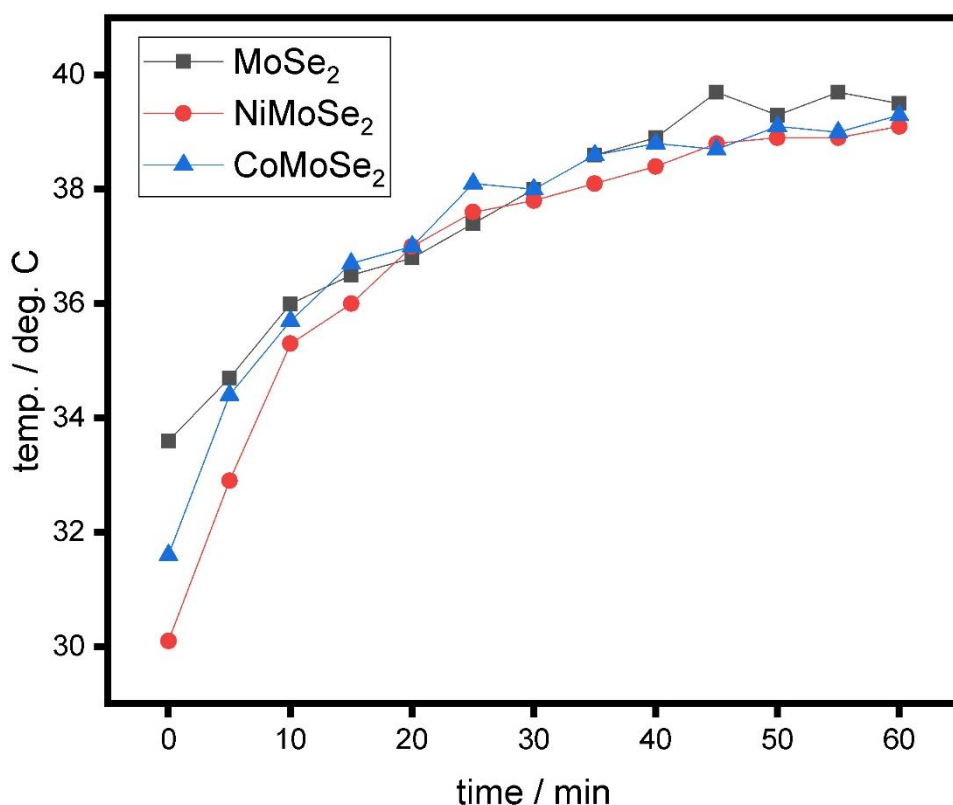


Figure 16: Photothermal efficiencies

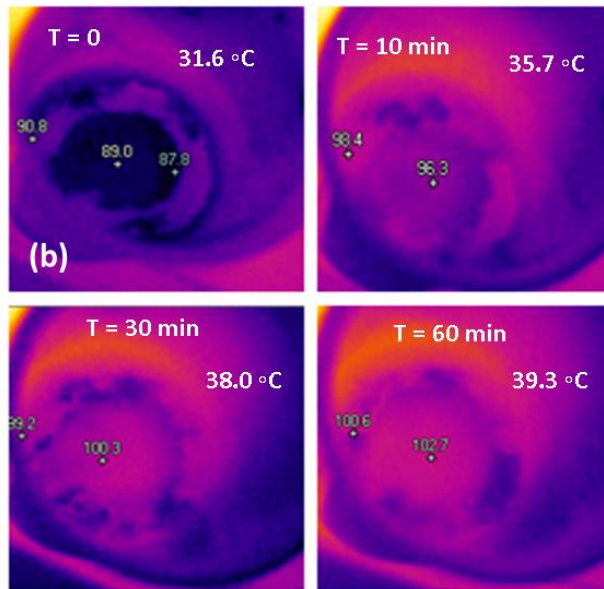
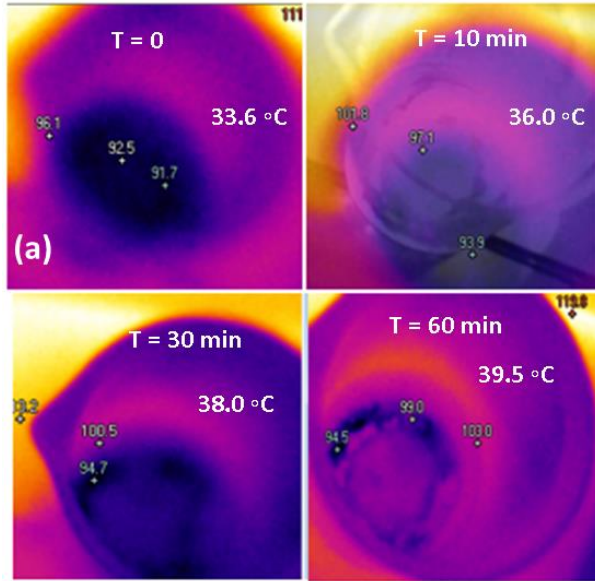
The effectiveness of photothermal conversion is displayed in IR photos of seawater taken at various time intervals. According to the graph, the interfacial temperature increased by around 1 °C in the first 10 minutes, 5 °C in 60 minutes, all of which indicate that the seawater exhibits a low photothermal conversion efficiency. In the center of the beaker, where the solar light is falling, is the hot zone. On the right side, a temperature scale is also displayed for temperature comparison. Every time an image was taken, the IR camera temperature scale was automatically adjusted to correspond with the object's temperature scale.

The temperature of the MoSe₂@CG membrane on the seawater's surface for solar desalination is depicted in the above figure. On the hot zone, the initial temperature is 33.6 °C. The MoSe₂@CG demonstrated good photothermal efficiency during the time. At intervals of five minutes, a rise in

temperature can be observed. The temperature increased to 39.5 °C after 60 minutes, demonstrating good photothermal efficiency as the surface temperature rose by 6 °C as a result of the membrane presence. The figure above shows the hot zone. The temperature scale is visible when comparing the interfacial surface temperature of the same beaker at various intervals.

The temperature of the CoMoSe₂@CG membrane on the seawater surface for solar desalination is depicted in the above figure. On the hot zone, the initial temperature is 31.6 °C. The CoMoSe₂@CG demonstrated a better photothermal efficiency during the time. At intervals of five minutes, a rise in temperature was observed. The temperature increased to 39.3 °C after 60 minutes, demonstrating good photothermal efficiency as the surface temperature rose by 8 °C as a result of the membrane presence. The figure above shows the hot zone. The temperature scale is visible when comparing the interfacial surface temperature of the same beaker at various intervals.

NiMoSe₂@CG, which is remarkably the best material of those we have synthesized, demonstrated the best photothermal conversion efficiency with a solar efficiency of 94.9 %. The diagrams above show the surface temperatures. The temperature is 30.1° at the beginning; after 10 minutes, it has increased to 35.3°, demonstrating excellent photothermal conversion efficiency. The temperature reached a remarkable value of 37.8° within half an hour. The temperature on the surface gradually increased from 30 minutes to an hour as the compound had already achieved its maximum temperature.



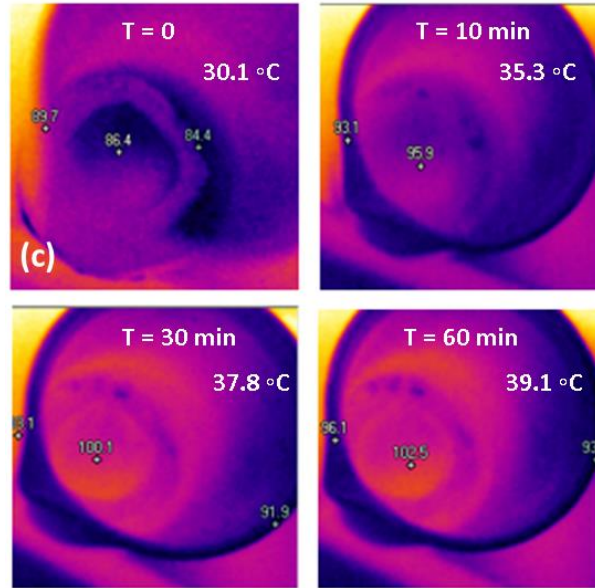


Figure 17: IR images of (a) MoSe_2 , (b) CoMoSe_2 and (c) NiMoSe_2

4.8 Stability

The stability of the synthesized substance was also tested on the prepared sample. The nanoparticle-coated membranes were employed for an hour under one sun irradiation. These membranes were then employed 3 more times for the same desalination procedure, and the results were consistent, demonstrating the stability of the produced membranes.

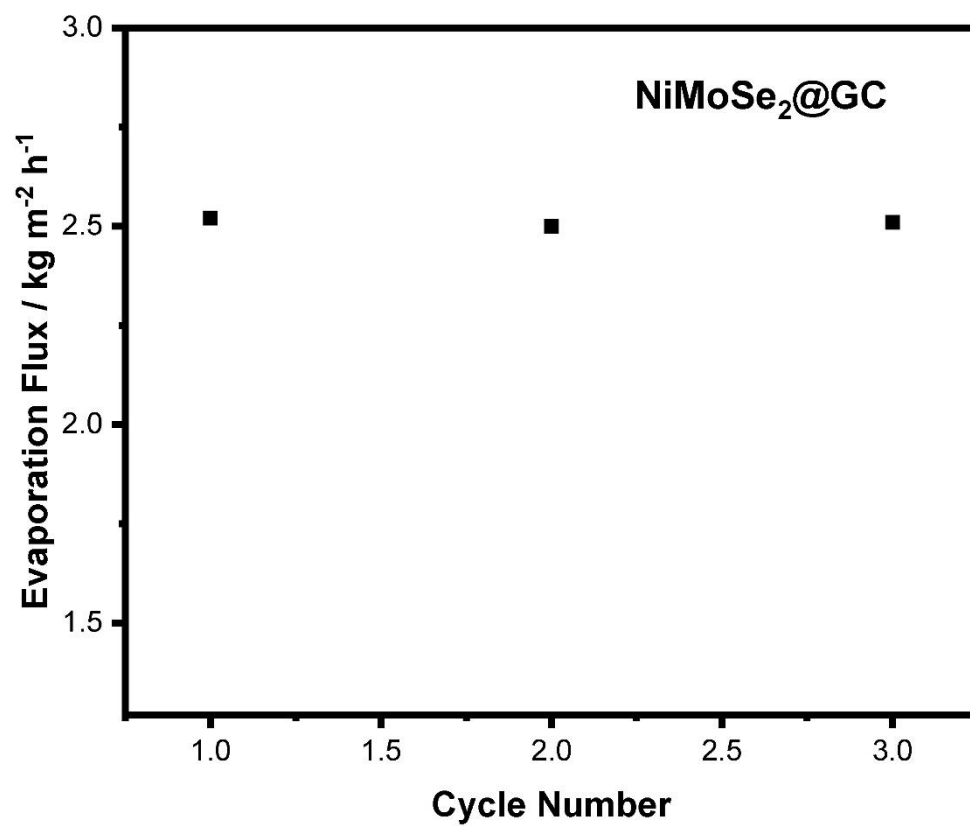


Figure 18: Stability Check

5. CONCLUSION

A porous, photothermal NiMoSe₂ based membrane was synthesized which exhibited excellent photothermal conversion efficiency for solar water evaporation. The nanoparticles were synthesized using hydrothermal method and deposited on the cotton gauze via ultrasonication. The nanoparticles showed the properties of low band gap energy, excellent stability, hydrophilicity, and low thermal conductivity which were responsible for light-to-heat conversion with a high solar efficiency. The evaporation rate shown by NiMoSe₂@CG was found to be 2.52 kg m⁻² h⁻¹ and the solar efficiency was calculated as 94.9 %. The evaporating device derived from cotton gauze and NiMoSe₂ nanoparticles is expected to produce clean water using solar energy.

6. REFERENCES

- [1] A. G. M. Ibrahim, A. M. Rashad, and I. Dincer, “Exergoeconomic analysis for cost optimization of a solar distillation system,” *Sol. Energy*, vol. 151, pp. 22–32, 2017, doi: 10.1016/j.solener.2017.05.020.
- [2] G. N. Tiwari, H. N. Singh, and R. Tripathi, “Present status of solar distillation,” *Sol. Energy*, vol. 75, no. 5, pp. 367–373, 2003, doi: 10.1016/j.solener.2003.07.005.
- [3] N. C. Darre and G. S. Toor, “Desalination of Water: a Review,” *Curr. Pollut. Reports*, vol. 4, no. 2, pp. 104–111, 2018, doi: 10.1007/s40726-018-0085-9.
- [4] S. Jiang, Y. Li, and B. P. Ladewig, “A review of reverse osmosis membrane fouling and control strategies,” *Sci. Total Environ.*, vol. 595, pp. 567–583, 2017, doi: 10.1016/j.scitotenv.2017.03.235.
- [5] P. Xu, T. Y. Cath, A. P. Robertson, M. Reinhard, J. O. Leckie, and J. E. Drewes, “Critical review of desalination concentrate management, treatment and beneficial use,” *Environ. Eng. Sci.*, vol. 30, no. 8, pp. 502–514, 2013, doi: 10.1089/ees.2012.0348.
- [6] M. M. Khairat Dawood, A. Amer, M. A. Teamah, A. Aref, and M. M. K. Dawood, “A Review Study of Experimental and Theoretical Humidification Dehumidification Solar Desalination Technology,” no. July, 2020, doi: 10.4236/cweee.2020.93005.
- [7] X. Luo, J. Shi, C. Zhao, Z. Luo, X. Gu, and H. Bao, “The energy efficiency of interfacial solar desalination,” *Appl. Energy*, vol. 302, no. May, p. 117581, 2021, doi: 10.1016/j.apenergy.2021.117581.
- [8] M. Shang *et al.*, “Full-Spectrum Solar-to-Heat Conversion Membrane with Interfacial Plasmonic Heating Ability for High-Efficiency Desalination of Seawater,” *ACS Appl.*

- Energy Mater.*, vol. 1, no. 1, pp. 56–61, 2018, doi: 10.1021/acsaem.7b00135.
- [9] S. Ai, M. Ma, Y. Z. Chen, X. H. Gao, and G. Liu, “Metal-ceramic carbide integrated solar-driven evaporation device based on ZrC nanoparticles for water evaporation and desalination,” *Chem. Eng. J.*, vol. 429, no. August 2021, p. 132014, 2022, doi: 10.1016/j.cej.2021.132014.
- [10] Y. Wang, J. Nie, Z. He, Y. Zhi, X. Ma, and P. Zhong, “Ti₃C₂T_xMXene Nanoflakes Embedded with Copper Indium Selenide Nanoparticles for Desalination and Water Purification through High-Efficiency Solar-Driven Membrane Evaporation,” *ACS Appl. Mater. Interfaces*, vol. 14, no. 4, pp. 5876–5886, 2022, doi: 10.1021/acsaami.1c22952.
- [11] Y. Lu *et al.*, “Fe₂O₃ nanoparticles deposited over self-floating facial sponge for facile interfacial seawater solar desalination,” *Crystals*, vol. 11, no. 12, pp. 1–14, 2021, doi: 10.3390/cryst11121509.
- [12] Y. Zhao, D. You, W. Yang, H. Yu, Q. Pan, and S. Song, “Cobalt nanoparticle-carbon nanoplate as the solar absorber of a wood aerogel evaporator for continuously efficient desalination,” *Environ. Sci. Water Res. Technol.*, vol. 8, no. 1, pp. 151–161, 2022, doi: 10.1039/d1ew00593f.
- [13] Y. Liu *et al.*, “A high-absorption and self-driven salt-resistant black gold nanoparticle-deposited sponge for highly efficient, salt-free, and long-term durable solar desalination,” *J. Mater. Chem. A*, vol. 7, no. 6, pp. 2581–2588, 2019, doi: 10.1039/c8ta10227a.
- [14] J. Yao and G. Yang, “An efficient solar-enabled 2D layered alloy material evaporator for seawater desalination,” *J. Mater. Chem. A*, vol. 6, no. 9, pp. 3869–3876, 2018, doi: 10.1039/c7ta10832j.

- [15] X. Wang, Y. He, X. Liu, G. Cheng, and J. Zhu, “Solar steam generation through bio-inspired interface heating of broadband-absorbing plasmonic membranes,” *Appl. Energy*, vol. 195, pp. 414–425, 2017, doi: 10.1016/j.apenergy.2017.03.080.
- [16] H. Li, Y. He, Z. Liu, B. Jiang, and Y. Huang, “A flexible thin-film membrane with broadband Ag@TiO₂ nanoparticle for high-efficiency solar evaporation enhancement,” *Energy*, vol. 139, pp. 210–219, 2017, doi: 10.1016/j.energy.2017.07.180.
- [17] L. Zhou *et al.*, “3D self-assembly of aluminium nanoparticles for plasmon-enhanced solar desalination,” *Nat. Photonics*, vol. 10, no. 6, pp. 393–398, 2016, doi: 10.1038/nphoton.2016.75.
- [18] H. D. Kiriarachchi, F. S. Awad, A. A. Hassan, J. A. Bobb, A. Lin, and M. S. El-Shall, “Plasmonic chemically modified cotton nanocomposite fibers for efficient solar water desalination and wastewater treatment,” *Nanoscale*, vol. 10, no. 39, pp. 18531–18539, 2018, doi: 10.1039/c8nr05916k.
- [19] A. Manuscript, “Nanoscale,” 2017, doi: 10.1039/C7NR05149B.
- [20] C. Yoo *et al.*, “Journal of Water Process Engineering 2D MoS₂-polyurethane sponge for solar-to-thermal energy conversion in environmental applications : Crude oil recovery and seawater desalination,” *J. Water Process Eng.*, vol. 47, no. November 2021, p. 102665, 2022, doi: 10.1016/j.jwpe.2022.102665.
- [21] L. Zhao, Q. Yang, W. Guo, H. Liu, and F. Qu, “Co₂S₄-Based Photothermal Membrane with High Mechanical Properties for Efficient Solar Water Evaporation and Photothermal Antibacterial Applications,” 2019, doi: 10.1021/acsami.9b04452.

- [22] J. Wang *et al.*, “High-Performance Photothermal Conversion of Narrow-Bandgap Ti₂O₃ Nanoparticles,” pp. 1–6, 2017, doi: 10.1002/adma.201603730.
- [23] B. Zhu *et al.*, “Flexible and Washable CNT-Embedded PAN Nonwoven Fabrics for Solar-Enabled Evaporation and Desalination of Seawater,” 2019, doi: 10.1021/acsami.9b12806.
- [24] S. Vafakhah *et al.*, “Tungsten disulfide-reduced GO / CNT aerogel: a tuned interlayer spacing anode for efficient water,” pp. 10758–10768, 2021, doi: 10.1039/d1ta01347e.
- [25] K. Gethard, O. Sae-khow, and S. Mitra, “Water Desalination Using Carbon-Nanotube-Enhanced Membrane Distillation,” pp. 110–114, 2011.
- [26] L. Li, L. Zang, S. Zhang, T. Dou, X. Han, and D. Zhao, “Journal of the Taiwan Institute of Chemical Engineers GO / CNT-silica Janus nanofibrous membrane for solar-driven interfacial steam generation and desalination,” *J. Taiwan Inst. Chem. Eng.*, vol. 111, pp. 191–197, 2020, doi: 10.1016/j.jtice.2020.03.015.
- [27] R. Article, Y. Xu, J. Yin, J. Wang, and X. Wang, “Design and optimization of solar steam generation system for water purification and energy utilization: A review,” pp. 226–247, 2019.
- [28] C. Chen *et al.*, “Highly Flexible and Efficient Solar Steam Generation Device,” *Adv. Mater.*, vol. 29, no. 30, pp. 1–8, 2017, doi: 10.1002/adma.201701756.
- [29] M. Zhu *et al.*, “Plasmonic Wood for High-Efficiency Solar Steam Generation,” *Adv. Energy Mater.*, vol. 8, no. 4, pp. 1–7, 2018, doi: 10.1002/aenm.201701028.
- [30] Y. Yang *et al.*, “Graphene-Based Standalone Solar Energy Converter for Water Desalination and Purification,” *ACS Nano*, vol. 12, no. 1, pp. 829–835, 2018, doi:

10.1021/acsnano.7b08196.

- [31] Y. Shi, O. Ilic, H. A. Atwater, and J. R. Greer, “All-day fresh water harvesting by microstructured hydrogel membranes,” *Nat. Commun.*, vol. 12, no. 1, pp. 1–10, 2021, doi: 10.1038/s41467-021-23174-0.
- [32] Y. Wang, C. Wang, X. Song, S. K. Megarajan, and H. Jiang, “A facile nanocomposite strategy to fabricate a rGO-MWCNT photothermal layer for efficient water evaporation,” *J. Mater. Chem. A*, vol. 6, no. 3, pp. 963–971, 2018, doi: 10.1039/c7ta08972d.
- [33] P. Zhang, J. Li, L. Lv, Y. Zhao, and L. Qu, “Vertically Aligned Graphene Sheets Membrane for Highly Efficient Solar Thermal Generation of Clean Water,” *ACS Nano*, vol. 11, no. 5, pp. 5087–5093, 2017, doi: 10.1021/acsnano.7b01965.
- [34] J. Han, Z. Dong, L. Hao, J. Gong, and Q. Zhao, “Poly(ionic liquid)-crosslinked graphene oxide/carbon nanotube membranes as efficient solar steam generators,” *Green Energy Environ.*, vol. 8, no. 1, pp. 151–162, 2023, doi: 10.1016/j.gee.2021.03.010.
- [35] X. Wu *et al.*, “A flexible photothermal cotton-CuS nanocage-agarose aerogel towards portable solar steam generation,” *Nano Energy*, vol. 56, no. October 2018, pp. 708–715, 2019, doi: 10.1016/j.nanoen.2018.12.008.
- [36] Z. Li *et al.*, “Arched Bamboo Charcoal as Interfacial Solar Steam Generation Integrative Device with Enhanced Water Purification Capacity,” *Adv. Sustain. Syst.*, vol. 3, no. 4, pp. 1–10, 2019, doi: 10.1002/adsu.201800144.
- [37] K. Fang, C. Du, J. Zhang, C. Zhou, and S. Yang, “Molecular engineering of a synergistic photocatalytic and photothermal membrane for highly efficient and durable solar water

- purification,” *J. Memb. Sci.*, vol. 663, no. September, p. 121037, 2022, doi: 10.1016/j.memsci.2022.121037.
- [38] J. Jiang, H. Jiang, Y. Xu, M. Chen, and L. Ai, “Janus Co@C/NCNT photothermal membrane with multiple optical absorption for highly efficient solar water evaporation and wastewater purification,” *Colloids Surfaces A Physicochem. Eng. Asp.*, vol. 647, no. April, p. 128960, 2022, doi: 10.1016/j.colsurfa.2022.128960.
- [39] X. Ren, S. Cui, J. Guan, H. Yin, H. Yuan, and S. An, “PAN@PPy nanofibrous membrane with core-sheath structure for solar water evaporation,” *Mater. Lett.*, vol. 313, no. November 2021, p. 131807, 2022, doi: 10.1016/j.matlet.2022.131807.
- [40] S. Ramaraj, M. Sakthivel, S. M. Chen, and K. C. Ho, “Active-Site-Rich 1T-Phase CoMoSe₂ Integrated Graphene Oxide Nanocomposite as an Efficient Electrocatalyst for Electrochemical Sensor and Energy Storage Applications,” *Anal. Chem.*, vol. 91, no. 13, pp. 8358–8365, 2019, doi: 10.1021/acs.analchem.9b01152.
- [41] K. Ai, J. Huang, Z. Xiao, Y. Yang, Y. Bai, and J. Peng, “Localized surface plasmon resonance properties and biomedical applications of copper selenide nanomaterials,” *Mater. Today Chem.*, vol. 20, 2021, doi: 10.1016/j.mtchem.2020.100402.